Implementation and Inspection of a High-Cycle Accumulation Model

Thesis Report

by

Thijs L. Lukkezen

Master of Science
in Civil Engineering

Thesis committee:	Prof. dr. M. A. Hicks,	TU Delft
	Dr. ir. P. Hölscher,	TU Delft, Deltares
	Drs. G. A. van den Ham,	Deltares
	Dr. F. Pisanò,	TU Delft
	Dr. ir. R.B.J. Brinkgreve,	TU Delft

ACKNOWLEDGEMENTS

Before you lies the result of the hard work during my graduation internship at Deltares. My graduation track has not been a smooth ride, but was rather a bumpy road from beginning to the end, filled with challenges, dead ends, new beginnings, but also satisfaction when things finally worked out. Of course, I could not have done this simply on my own and therefore there are a couple of people that I would like to thank in particular. First of all, I would like to thank my daily supervisors at Deltares: Paul H olscher and Geeralt van den Ham. Thank you both for the pleasant meetings and coffee breaks we had where you gave me plenty of valuable advice on my thesis, but I also enjoyed our chats on non-thesis related topics. Next I would like to thank Vahid Galavi and Jonathan Nuttal from Deltares for your support with the Plaxis implementation. I have asked plenty of your time and knowledge on Plaxis UDSM routines and Fortran programming language, of which I am absolutely thankful. I would also like to thank Andrzej Niemunis for providing me the UMAT code of the HCA model and Torsten Wichtmann for our correspondence and the very useful advice and answers to my many questions about the HCA model. Also a warm thanks to Ronald Brinkgreve, Michael Hicks and Federico Pisanò for joining the committee on behalf of the TUD and providing me with feedback and guidance during the various meetings we had. Furthermore I would like to thank all other persons who helped me out at Deltares on smaller and bigger issues; the Deltares graduation student community who provided a welcome distraction during the lunch and coffee brakes; my roommates, who provided a listening ear to my incomprehensible gibberish during times of stress and were always there to cheer me up; and my other friends and family who supported me through the process in many ways.

Thijs L. Lukkezen
Delft, June 2016

ABSTRACT

The prediction of permanent deformation accretion in granular materials as a result of long-term cyclic loading is a complex challenge that receives great attention in engineering fields, including infrastructural design and design of offshore wind turbines. Many models have been proposed in the past which aim to predict this cyclic deformation accumulation for specific or general purpose. One of the most advanced models available is the "High-Cycle Accumulation (HCA) model" by Niemunis et al (2005) [1]. Although very promising, this model is as of yet rarely used in Dutch geotechnical engineering practice. One of the possible reasons for this is the lack of understanding and availability of the model. This thesis has the aim to overcome these problems by gathering relevant information on the HCA model, implementing it in Plaxis 2D finite element software and inspecting the capabilities of the resulting FE routine. After gathering the information on the model from literature, it was concluded that the model has great potential and is the most extensively validated model available. However, there are also some boundary conditions for which the model fails to predict the deformations correctly. The model also requires a vast number of advanced laboratory tests to be carried out in order to compute the model parameters.

The implementation of the constitutive equations in Plaxis 2D was performed successfully and was verified for a single-element type case. When applying the FE routine to a boundary value problem, numerical issues arising from the finite element calculation kernel conflict with the sensitivity of the HCA model to the state parameters, resulting in a severe over-estimation of accumulated settlements. A sensitivity analysis was carried out, which shows that the model is highly sensitive to the parameters of the hypoplastic model (which is used in the initial calculation phase of the FE routine). It is concluded that for the HCA routine to be used in Plaxis, the numerical issues should be investigated and possibly a numerical interface should be designed. The high sensitivity to the model parameters, combined with the vast amount of required effort (and cost) to compute these parameters for a sand sample make the model less favourable for practical design applications.

CONTENTS

LIST OF FIGURES

LIST OF TABLES

1
INTRODUCTION

1.1. GENERAL CONTEXT

One particular type of problems in the field of geo-engineering rises from variable loads with a cyclic recurrence pattern, also called 'cyclic loads'. Cyclic loads in geo-engineering can be caused by objects or other sources which exert periodically variable forces on a soil body. One can think of the loads on foundations of structures which vibrate in the wind such as wind turbines or pillars of high bridges; levees which experience wave loading and tidal influences; foundations for sea locks with large variations in water level; and road or rail embankments which experience peak forces with each passing car or train. Special attention is given to cyclic loading with sand. Sand is not a rigid material, so the grains can move with respect to each other. The required effort to put the grains in motion is dependent on the material characteristics of the sand, the shape of the grain skeleton and the local stress states. Each cyclic load can cause small deformations in the sand skeleton. If the movement of the particles causes them to move more closely together, the sand will reach a denser configuration (a process called compaction). Alternatively, the grains can reach a looser configuration (called dilatancy) if they move away from each other.

Compaction and dilatancy can have various desired or undesired side-effects. A densely packed sand will, for instance, have better strength properties than a loosely packed sand and compaction can therefore be thought of as a good thing. However, compaction and dilatancy will also lead to a change of the soil volume, which can cause subsidence or heave of the soil surface. These effects may be undesired for adjacent foundations of structures. When the pore space (the space between the sand grains) is filled with a fluid, compaction can lead to undesired complex phenomena like liquefaction, leading to a (temporary) reduction of the soil strength.

Cyclic loading is an important concept to many of the discussed models and problems in this thesis. It is important to distinguish between static, cyclic and dynamic loads since they all require a different approach in engineering practice. Strictly speaking, there is no fundamental difference between the types of loading, other than the time dependency of the load magnitude. On the other hand, the reactive behaviour of the soil varies significantly with each loading type, which underlines the importance of the classification. The type of analysis (static/cyclic/dynamic) that is required depends on the time dependency of the loading and the composition, weight, stiffness and strength characteristics of the soil. When only the self-weight of a structure is considered as a load on the foundation, no time dependency is expected since the structure will maintain a constant weight under normal conditions. The questions to be answered in this consideration are related to the static failure mechanisms of the soil. When the magnitude of the load is expected to be time dependent, cyclic or dynamic effects could be considered. Dynamic effects could play a role when the speed of change of the load magnitude is relatively high, considering the soil damping, unit weight and stiffness properties. The calculation of the soil accelerations is a key component of a dynamical analysis since they can impose large fluctuations in stress levels or severely disrupt the stability of the soil. When the change in load magnitude happens relatively slowly and follows a recurring pattern, cyclic effects may be considered. The continued variation in loading may, over time, lead to changes in the soil structure and the stiffness and strength characteristics of the soil, as described in

the previous section. The resistance against static failure may be influenced by these changes. This analogy is similar to the one used in steel fatigue engineering [11, 12].

The changes in the soil structure are often referred to as deformations (i.e. the absolute spatial value) or strains (i.e. deformation relative to the material dimension). Deformations in sand take place on a small scale (compression, rotation, translation and abrasion of the sand grains) where they may seem irrelevant, but the combined effect of all small scale deformations can have a noticeable effect on a larger scale (subsidence or even collapse of the soil surface). A distinction is often made between elastic (reversible) and plastic (irreversible) deformations. When, for instance, a certain load on a soil causes a deformation that vanishes once the load is removed, this deformation is considered to be purely elastic. However, when a certain amount of deformation remains after removal of the load, this remaining deformation is referred to as the plastic deformation. Elastic deformation is thought to be caused mostly by compression of the soil skeleton with little movement of the grains (i.e. the grain structure stays mostly in tact). Plastic deformation is thought to occur when the grains start translating or rotating with respect to each other or when grain crushing occurs. In these cases, the grain structure reaches a new equilibrium configuration and will not naturally fall back to the previous state. It is important to notice that in reality the plastic and elastic deformations often occur together and are not so easily distinguished. However, it is thought that strains that are smaller than a certain threshold value, are purely in the elastic regime (a threshold strain of around $1 \cdot 10^{-4}$ is generally adopted in literature [13, 14]) A Cyclic loading with small recurring deformations in the elastic regime, however, can lead to plastic deformations over the course of a large number of cycles, which is the fundamental idea of cyclic strain accumulation [15].

Since the 1970's, various attempts have been made by engineers and scientists to design a model with which a prediction can be made of the deformation of a granular material (like sand) that is subjected to cyclic loading. A distinction is made between models that describe the complete stress-strain response of a material and semi-empirical models that only calculate the accumulation of plastic strains. The first group of models is usually not specifically designed to deal with cyclic loading and the use of such models for this purpose can result in extensive calculation times and large uncertainties [1]. The latter group of models are called compaction models or accumulation models since they take into account the accumulated deformations of each load cycle. Many of these models were designed for a specific purpose, such as road or railway engineering. These models have intrinsic assumptions about the stress state or other boundary conditions [16–19]. A few models have been posed with the aim to be applicable to a broader band of engineering problems [1, 20–22]. All accumulation models are highly empirical, since the basic relationships are based on (laboratory) observations, rather than a deeper understanding of the underlying mechanisms. In chapter 2, a more detailed overview is provided of the currently available accumulation models.

One of the currently developed and most advanced models available is the Bochum accumulation model, also referred to as the High-Cycle Accumulation (HCA) model, by Niemunis et al. [1]. It is the only model which is aimed to provide volumetric and deviatoric strain accumulation predictions for a (very) large number of load cycles of an arbitrary source, which is validated with laboratory tests with up to two million load cycles. It was concluded by Wichtmann [15] and Wichtmann et al. [8, 23, 24] that the magnitude and direction of strain accumulation is sensitive to the shape and size of the cyclic strain path, (variations in) average stress state, history of cyclic loading and the initial, current and terminal density of the granular material. Other models do not correctly take the combination of these important features into account and the HCA model is therefore thought to be the most accurate and advanced for a wide range of applications.

1.2. JUSTIFICATION OF RESEARCH

Despite the seemingly promising capabilities of the HCA model, not much experience has been gained with it in Dutch geotechnical engineering society. One of the reasons for this can be that the

model is still relatively new and research on the topic is far from finished. Another reason might be the lack of availability. Most Dutch geotechnical engineers prefer to work with the geotechnical FE software Plaxis, rather than Abaqus. At knowledge institute Deltares and Delft University of Technology, researchers and engineers share a curiosity for the capabilities of the HCA model but are reluctant to use it. Providing access to the model by making it available in Plaxis might open the door to new possibilities. Dutch geotechnical engineers and researchers might then choose to use it to solve engineering problems or contribute to scientific research.

Predictions of compaction of a sandy subsoil as a result of cyclic loading are currently subject to large uncertainties. Decreasing the degree of uncertainty can be of large economic value for the design of structures with a low margin for soil settlements. One can, for instance, think of offshore and onshore wind turbine farms or high-speed railway tracks.

1.3. OBJECTIVES & METHODOLOGY

The main objectives for this thesis are:

- Increase the availability of the HCA routine to geotechnical engineers and scientist in The Netherlands.
- Identify the possibilities and limitations of applying the HCA model in a Plaxis finite element routine for a relevant engineering problem and formulate recommendations for future use.

To achieve the main objectives, the following actions were proposed:

- Performing a literature study to get a state-of-the-art overview of the theoretical framework and experiences gained with the model.
- Implementation of the HCA model in Plaxis 2D FE software by writing a UDSM in Fortran programming language. The UDSM shall be based on the Abaqus UMAT implementation, for which a so called "wrapper" must be written.
- Recalculation of long-term cyclic triaxial test calculations in Plaxis 2D.
- Validation of the HCA routine in Plaxis 2D by recalculating the results of a shallow foundation centrifuge test.

1.4. THESIS OUTLINE

In chapter 2 the main concept of cyclic strain accumulation models is provided, together with an overview of the well established available models, some of which are discussed more thoroughly.

The workings of the HCA model by Niemunis et al. are elaborated on thoroughly in chapter 3. A detailed description is provided, combined with new insights from the late ten years of research and some known applications are discussed. Also a modified and extended version of the hypoplasticity model is described briefly there.

In chapter 4 the implementation of the HCA model in Plaxis 2D FE software is discussed, together with some necessary model adjustments.

To check whether the implementation of the HCA model was performed correctly, a verification procedure was executed, which is discussed in chapter 5.

A recalculation of a shallow foundation centrifuge tests was performed, as a means to validate the implemented routine and inspect the possibilities and draw-backs. This is described in chapter 6.

Finally, the main conclusions and recommendations of the thesis are described in chapter 7.

2

CURRENT MODELS AND PRACTICES

Since the 1980's, various attempts have been made by engineers and scientists to design a model with which a prediction of the amount of compaction of a granular material (like sand) that is subjected to cyclic or dynamic loading can be made. Such models are called compaction models or accumulation models since they take into account the accumulated plastic deformations of each load cycle.

2.1. GENERAL CONCEPT

To illustrate the general concept of cyclic accumulation models, let us first look at a general definition for stresses and strains. Consider a rigid square box filled with sand. The height of the sand in the box is L. When a uniform vertical stress σ is applied to the surface (for instance with a hydraulic press), the sand will deform with a vertical deformation u, as is illustrated in Figure 2.1. The vertical deformation of the sand can be expressed as a (dimensionless) strain ε by division by the original height of the sample: $\varepsilon = u/L$. The amount of straining caused by the applied stress will depend on the magnitude of the stress and the stiffness properties of the sand. In the rest of this example, it can be assumed that the applied stress is relatively small and so the displayed deformation u in Figure 2.1 is extremely exaggerated. In reality it will be barely noticeable to the human eye. In this regime of small stresses and deformations, sand is generally considered to behave like a linear elastic material[1].

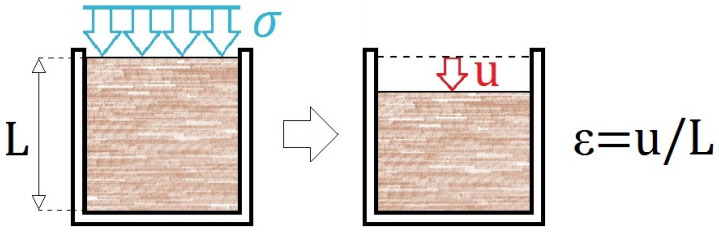

Figure 2.1: Thought experiment: square box filled with sand subjected to a uniform vertical pressure.

One can imagine that when the applied vertical stress is increased, also the vertical strain will increase. If thereafter the stress is reduced to the previous level, one might expect the strains to also return to the previous level, since it was assumed that the sand will bounce back elastically. But in reality, a small irreversible deformation has been made by the application of the stress[2] which prevents the sand to bounce back to its original level completely. The increase and decrease of the stress level can be seen as a load cycle. The vertical strain ε resulting from each load cycle can be

[1] Which means that a linear relation exists between the applied stress and the resulting strain: $\sigma = E \cdot \epsilon$, where E is the modulus of elasticity (Young's modulus) of the sand.

[2] The true process leading to the irreversible strains is complex and not yet fully understood. Some of the grains may have rotated slightly or have moved with respect to each other.

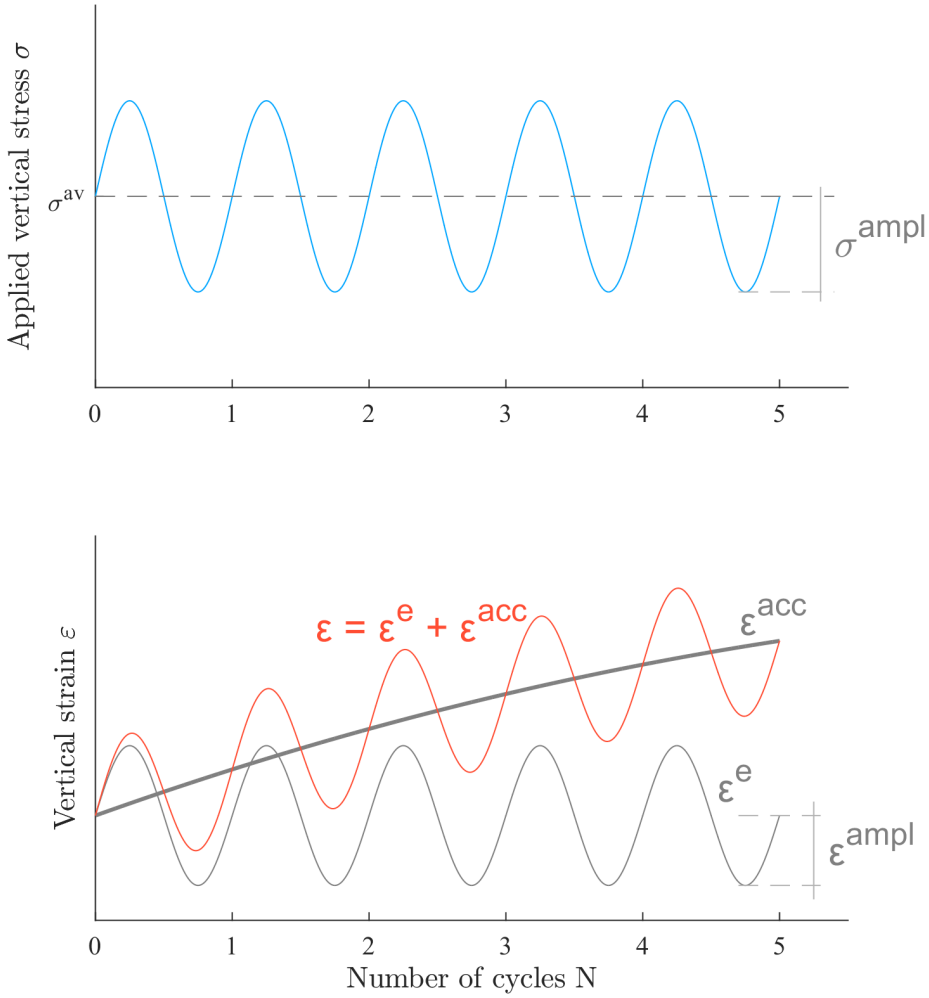

Figure 2.2: Evolution of ε, ε^{ampl} and ε^{c} (lower graph) during application of σ (upper graph).

decomposed in a cyclic (elastic) part ε^e and an accumulated (plastic) part ε^{acc} as can be seen in Figure 2.2. The fundamental idea of the strain accumulation is that a load cycle with a relatively small strain amplitude leads to very small irreversible strains. Over the course of only several cycles this effect is barely noticeable, but given a large number of cycles, the accumulation can lead to significant strains. Note that the example above is a highly simplified version of reality, meant to illustrate the main principal. The example only considers 1 component of the Cauchy stress state (vertical normal stress). In a realistic 3D situation, all six components of the Cauchy stress can be affected by cyclic loading.

Conventional soil models use an implicit scheme to calculate the total strain trajectory (the red line in Figure 2.2). This approach, however, can both be very time consuming and provide inaccurate results if hundreds of subsequent load cycles are to be considered (let alone millions of cycles!). Cyclic accumulation models have a different approach: Instead of calculating the total strain ε implicitly in real-time, they calculate the accumulated plastic strain (dark gray line in Figure 2.2) ε^{acc} explicitly in pseudo-time[3]. The approach is very similar to viscoplastic models, where instead of the time t, the number of cycles N is used. Due to the explicit formulation, large N-intervals can be calculated without a loss of accuracy. The explicit formulations have an empirical character, since

[3]Pseudo-time means some other unit than time is used with respect to which the model progresses. In this case, the number of cycles N is used as such unit.

they are mainly formed by fitting mathematical expressions to observed laboratory results.

2.2. TYPES OF ACCUMULATION MODELS

In chapter 1, a deviation was made between models that were designed for a specific engineering problem and those that approach the strain accumulation in a more general sense. Pasten et al [25] divided them in three categories, based on the output of the model and the considered state parameters which influence that output:

1. Models that only consider one part of accumulated deformation (volumetric/deviatoric) by taking into account the first load cycle (magnitude), cyclic history, static stress state and initial density. Examples are Diyaljee & Raymond 1982 [26], Gidel et al. 2001 [27], Lentz and Baladi 1981 [28], Sawicki 1987 [21], Sweere 1990 [29].

2. Models that only consider one part of accumulated deformation by taking into account a reference number of cycles, the static stress state and static shear strength: Barksdale 1972 [16], Brown 1974 [30], Lekarp & Dawson 1998 [19].

3. Models that consider the complete strain accumulation (volumetric and deviatoric) by taking into account the number of cycles, load magnitude, stress state and initial density: Bouckovalas et al. 1984 [31], François et al 2009 [22], Kaggwa et al. 1991 [32], Niemunis et al 2005 [1], Suiker & de Borst 2003 [18], Pasten et al. 2014 [25].

The models in the third group can be considered the most advanced models available, most of which can easily be implemented in FE routines, according to the authors. The models inside a group can still have very different bases and approaches, as can be seen in the following short elaborations on some of the models mentioned above.

2.3. SAWICKI

One of the early models which aimed to predict the compaction of granular soils due to cyclic shearing for general engineering problems was proposed by Sawicki in 1987 [21, 33]. The field of cyclic soil behaviour was still rather new back then, as the first studies that looked at the 'new' phenomena such as cyclic compaction and liquefaction date from the 1960's – with for instance the work of Seed and Lee [34] – but really only took off in the mid 1970's [33].

Sawicki's model [21, 33] was designed to predict the "compaction" ($\Phi = \Delta n / n_0$, with porosity n) of a fine sand based on the applied shear strain amplitude γ^{ampl} and the number of load cycles N:

$$\Phi \sim \ln(\tilde{N}), \tag{2.1}$$

where $\tilde{N}$ is a function of the number of cycles N and the shear strain amplitude γ^{ampl}. The possible influence of the average stress level or the shape of the cyclic strain path are not taken into account. Also, the deviatoric strain accumulation is not considered, since the definition of compaction only regards the volumeteric strain. The reducing effect of the initial density on the strain accumulation is taken into account, however the density is not updated during calculation. The intrinsic assumption of Equation 2.1 is that there exists a "common compaction curve" (see Figure 2.3), which is able to express the relationship between Φ and $\tilde{N}$, independent of the choice of applied shear stress amplitude γ^{ampl}. This assumption was confirmed with scale tests with up to 1000 cycles, however, has later been disproven by Wichtmann in [15] for values of $\tilde{N} > 1 \cdot 10^{-7}$.

2.4. SUIKER & DE BORST

Suiker & de Borst [18] proposed a model to simulate the cyclic deterioration of railway tracks. Railway tracks are usually founded on several layers of granular material, which are susceptible to settlements as a result of the repetitive loads from passing trains. The model calculates the accumulated

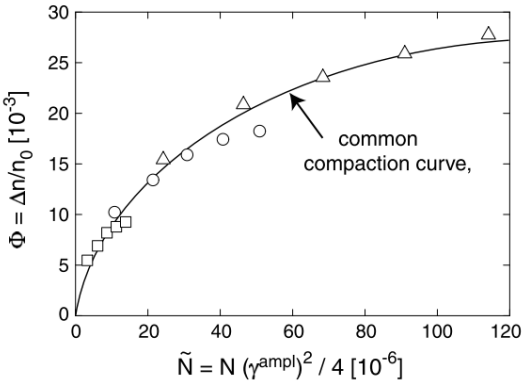

Figure 2.3: The common compaction curve of Sawicki's model compared to observations from lab tests. A fixed relationship is assumed between Φ, N and γ^{ampl} for every sand sample.

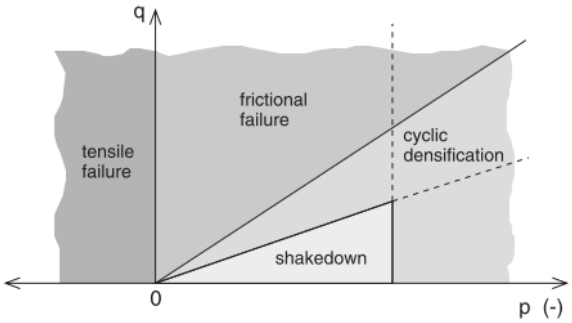

Figure 2.4: The four stress regimes of the model of Suiker & de Borst, each defining specific soil behaviour.

plastic strain, which is composed of a volumetric part (analogously to Sawicki's 'compaction') and a deviatoric part. It is assumed that the two parts are caused by the volumetric compacting and frictional sliding deformation mechanisms respectively.

The calculation of strain accumulation is mostly based on the peak stress state, which is composed of the static stress (due to own-weight and monotonic overburden forces) and the maximal additional overburden stress during cyclic loading. The model deviates between elastic straining and plastic strain accumulation by defining four stress regimes: *elastic shakedown*; *cyclic densification*; *frictional failure* and; *tensile failure*, which can be observed in Figure 2.4. When the stress state is in the elastic shakedown regime, only elastic straining is assumed. This reflects the underlying assumption that for cyclic loading beneath a threshold stress amplitude, no accumulation of plastic strains is expected. A pressure dependent elastic stiffness tensor controls the soil behaviour in this regime. A yield surface defines the transition between elastic and plastic compaction behaviour. This surface consists of a Drucker-Prager yield cone with compression cap. As the stress state enters the cyclic densification regime, the plastic strain accumulation is calculated. As the yield surface moves outward during cyclic loading, the stress state will eventually end up in the elastic shakedown regime which results in a maximal value of accumulated deformation after a certain number of cycles. When the stress state enters the frictional or tensile failure regime, plastic strains are calculated due to static failure of the soil. A series of model parameters are to be determined based on laboratory tests and engineering judgment.

The fact that the rate of plastic strain accumulation is only based on the maximum overburden stress means that the average stress and cyclic load amplitude are not taken into account. Furthermore, the void ratio is not considered as a state parameter that influences the strain accumulation.

2.5. FRANÇOIS ET AL.

The model of François et al. [22] is largely based on the model of Suiker & de Borst. But instead of predicting the settlement of the railtrack *itself*, the model can be used to predict the settlements of adjacent buildings which are affected by the dynamic wave loads resulting from the track. The static forces below a building are much larger than below a railway track, which is why this model does deviate between static and cyclic stresses. Since the model is meant to calculate the effect of dynamic waves, the cyclic load part is taken into account by assuming a low amplitude incident wave field. The magnitude of this wave field throughout the problem geometry is first to be determined in a dynamic calculation with a suitable soil model in a FE calculation, or a rough estimation can be made.

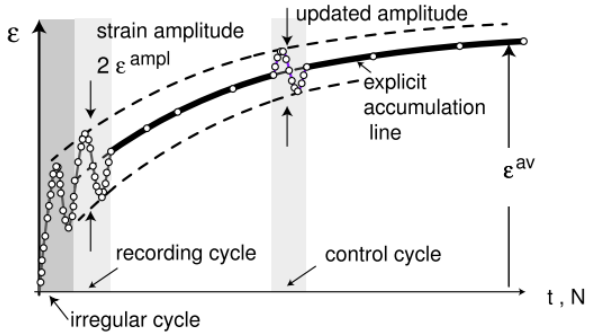

Figure 2.5: Basic concept of the HCA model [1].

2.6. NIEMUNIS ET AL.

The High-Cycle Accumulation (HCA) model by Niemunis et al. [1] builds on the same principles as Sawicki's model and is one of the most recent and advanced accumulation models available. It can be used to calculate the accumulation of strains and stresses in sand which is subject to small cyclic loading after a high number of cycles. The HCA model has been validated with a series of cyclic triaxial tests with up to 2 million load cycles. An implementation for the HCA model in the commercial software Abaqus has been written by the author of the model.

The HCA model requires the amplitude of cyclic straining as an input parameter. Since this amplitude is such an important parameter in the model, it needs to be determined accurately. Acquiring the amplitude from in-situ measurements is difficult for practical applications. The amplitude can, however, be calculated numerically with another soil model. The authors of the model suggest the use of the hypoplasticity model with intergranular strain extension. In Figure 2.5 this is illustrated as the recording cycle. Note that the first cycle of loading cannot be used, since the strain path is irregular and would provide a too large strain amplitude. After the recording cycle, the strain amplitude is determined and the accumulation with increasing number of cycles N can be calculated with the HCA model (the so called pseudo-creep phase). After a certain amount of cycles, the changes in density or stress state may have changed the strain amplitude. Therefore, the strain amplitude can be recalculated in a so-called 'control cycle'. An elaboration on the calculation phases and steps of the model can be found in section 3.1.

Cyclic loading of sand can lead to an accumulation of either deformations (pseudo-creep), or residual stresses (pseudo-relaxation), depending on the boundary conditions. Deformations in a sand body can occur due to compaction of the sand. However, when boundary conditions restrict straining (horizontal straining is, for instance, limited in an infinitely wide homogeneous sand body) a reduction of the stress state can occur. In practice, a combination of pseudo-creep and pseudo-relaxation effects can be observed simultaneously. For this reason, the term 'accumulation' refers to both the creep and relaxation parts.

The above explained mechanism of strain accumulations only applies to relatively small strain cycles. When the cyclic strain amplitude becomes too large, each load cycle will deform the grain structure, leading to an alternative deformation mechanism. Therefore, the HCA model can deal with total strain amplitudes of maximum $5 \cdot 10^{-3}$.

3

THE HIGH-CYCLE ACCUMULATION MODEL

In this chapter, the High-Cycle Accumulation model by Niemunis e.a. (2005) [1] is discussed. The introduction and general concept of the model are described in the last section of the previous chapter. The constitutive model with all components are discussed in the first section of this chapter. The properties of the model, which lay down the possibilities and limitations are discussed in the next chapter. Thereafter, the determination of the soil parameters is discussed in section 3.3 and some examples of usage in literature are provided thereafter. The hypoplasticity model, which is utilized in the HCA calculation routine, is discussed in section 3.5 and the chapter is concluded with a summary and discussion on the model.

3.1. CONSTITUTIVE MODEL

The basic constitutive equation of the HCA model [2] reads

$$\dot{\boldsymbol{\sigma}} = \mathbf{E} : \left(\dot{\boldsymbol{\varepsilon}} - \dot{\boldsymbol{\varepsilon}}^{acc} - \dot{\boldsymbol{\varepsilon}}^{pl} \right) \tag{3.1}$$

with the rate of effective stress $\dot{\boldsymbol{\sigma}}$, the elastic stiffness $\mathbf{E}$, the total strain rate ($\dot{\boldsymbol{\varepsilon}}$), accumulated strain rate ($\dot{\boldsymbol{\varepsilon}}^{acc}$), and plastic strain rate ($\dot{\boldsymbol{\varepsilon}}^{pl}$). A superscripted dot notation represents a derivation with respect to the number of cycles in throughout the rest of this document (e.g. $\dot{\boldsymbol{\varepsilon}} = \partial \boldsymbol{\varepsilon} / \partial N$).

A major difference between a conventional FE cyclic loading model and the one under consideration is that the conventional ones use implicit calculation, whereas this model calculates the accumulations explicitly [1] with respect to the pseudo-time N. This explicit character of the method is stored in the rate of accumulated strain $\dot{\boldsymbol{\varepsilon}}^{acc}$, which is the main element of the model (see subsection 3.1.1). An explicit calculation method for strain accumulation not only reduces analysis runtime, it also prevents inaccuracies due to the accumulation of numerical errors. These numerical errors in conventional methods can be of considerable magnitude when a high number of cycles is analysed [1].

The rate of plastic straining $\dot{\boldsymbol{\varepsilon}}^{pl}$ caused by monotonic loading is treated separately from $\dot{\boldsymbol{\varepsilon}}^{acc}$. Fundamentally, they cannot be regarded as different phenomena, but the separation results as a necessity from the explicit calculation strategy when implemented in an FE routine. Plastic strains can for instance result in case of two neighbouring cells with a different magnitude of accumulated straining. For their dimensions to match, a certain amount of plastic straining should be applied. The Matsuoka and Nakai [35] yield condition is used to calculate $\dot{\boldsymbol{\varepsilon}}^{pl}$. See subsection 3.1.3 for an elaboration on the plastic strain rate.

[1] 'Explicitly' refers to the fact that the increment of accumulation can be calculated explicitly for a given number of cycles N. Time step integration (i.e. Euler forward/backward) is not meant here.

The explicit FE method operates according to the following scheme:

Implicit phase

1. Calculation of the initial stress field (taking into account self-weight and static loads) using a conventional plasticity model. This step is only executed in the very beginning of the analysis.
2. Implicit (dynamic/pseudo-static) calculation of at least the first two load cycles, using a plasticity model where small strain non-linearity of soil is accounted for. The yield surface should not be encountered.
3. Recording of the logarithmic strain path during the first regular cycle at each integration point.
4. Evaluation of the tensorial strain amplitude A_ε from the recorded strain path in each integration point. This tensor is assumed constant in all of the following load cycles, until it is recalculated in a control-cycle.

Pseudo-creep phase

1. Calculation of the accumulation rate $\dot{\boldsymbol{\varepsilon}}^{acc}$ in every integration point according to (3.2). $\dot{\boldsymbol{\varepsilon}}^{acc}$ is calculated explicitly and is a function of A_ε, the current load cycle N and a selection of soil and stress state parameters. Some of these parameters are updated at the beginning of every calculation step and some follow from the initial conditions.
2. Calculation of the Cauchy stress rate $\dot{\boldsymbol{\sigma}}$ according to (3.1) and the stress increment $\Delta\boldsymbol{\sigma} = \dot{\boldsymbol{\sigma}}\,\Delta N$ caused by a loading block of ΔN cycles. The plastic strain rate $\dot{\boldsymbol{\varepsilon}}^{pl}$ – which may result from monotonic loading – is calculated according to the Matsuoka and Nakai yield condition.
3. The equilibrium condition is checked, i.e. the internal and external stresses are compared. If no equilibrium is reached, an iteration step is made by adjusting the stiffness matrix $\mathbf{E}$ and recalculating $\dot{\boldsymbol{\sigma}}$ in the previous step (this is the regular practice, required in FE methods).
4. Repetition of step 1-4 until: a new load block with different strain amplitude A_ε is reached (go back to step 2 of implicit phase); a control cycle is reached (continue); the end of the test is reached (stop).

Control phase In the control phase, the strain amplitude A_ε is recalculated according to steps 2-4 of the implicit phase. Afterwards, the Pseudo-creep phase can continue.

3.1.1. DECOMPOSITION OF THE ACCUMULATION RATE $\dot{\boldsymbol{\varepsilon}}^{acc}$

As mentioned before, the rate of accumulation $\dot{\boldsymbol{\varepsilon}}^{acc}$ is the essential part of the model. It is recalculated in each step according to

$$\dot{\boldsymbol{\varepsilon}}^{acc} = \mathbf{m}\, f_{amp}\, \dot{f}_N\, f_p\, f_Y\, f_e. \tag{3.2}$$

In this formula, $\mathbf{m}$ accounts for the direction of accumulation in strain space. The factors f_{amp}, $\dot{f}_N$, f_p, f_Y and f_e account for the influence of strain amplitude, the number of cycles N, the average stress ratio p^{av} and the void ratio e respectively. The composition of these factors will be elaborated on in the rest of this section.

Note that the frequency of cyclic loading is not taken into account in the calculation of the rate of accumulation. This was done since research by many authors (summarized in [23]) has concluded that cyclic frequencies in the range of 0.1 to 12 Hz have a negligible effect on the rate of accumulation for both drained and undrained conditions.

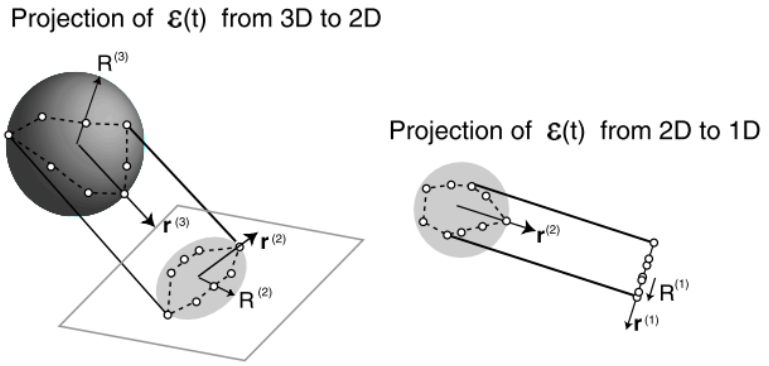

Figure 3.1: A visualization of the process with which the tensorial amplitude A_ε is derived from the strain path. A_ε consists of a set of directional vectors **r**, multiplied by their corresponding magnitudes **R**. In a 3-dimensional calculation, the strain space is 6-dimensional, which is rather hard to visualize, but the same principal as shown here are applied [1].

DIRECTION OF ACCUMULATION: m

The accumulation $\dot{\boldsymbol{\varepsilon}}^{acc}$ has both a volumetric and a deviatoric portion, the ratio of which is known as the direction of accumulation. It was found in [24, 36] that the direction of straining is mainly dependent on the average stress ratio $\eta = q/p$. Therefore a flow rule was adopted in (3.2) to approximate the direction of accumulation. In particular, the modified Cam-Clay flow rule

$$\mathbf{m} \sim -\frac{1}{3}\left(p - \frac{q^2}{M^2 p}\right)\mathbf{1} + \frac{3}{M^2}\boldsymbol{\sigma}^* \tag{3.3}$$

is used with Roscoe's invariants p and q and the critical state line $M = \frac{6\sin\varphi_c}{3\pm\sin\varphi_c}$.

SCALAR VALUE OF THE AMPLITUDE: f_{amp}

The magnitude of the strain amplitude $\hat{\varepsilon}$ (scalar) is an essential control parameter for $\dot{\boldsymbol{\varepsilon}}^{acc}$. It enters (3.2) via f_{amp}. The strain amplitude for arbitrary strain cycles can be found via the tensorial amplitude A_ε. This is a tensor, containing the principal directions and magnitudes of the strain amplitude which is derived from the recorded strain path, as illustrated in Figure 3.1. The scalar value of the strain amplitude is found by taking the euclidean norm of the tensorial strain amplitude. A linear relationship between the accumulation rate and a power law of the amplitude holds up to strain amplitudes of 10^{-3}. Therefore f_{amp} is calculated with

$$f_{amp} = \begin{cases} \left(\frac{\hat{\varepsilon}}{\hat{\varepsilon}_{ref}}\right)^{C_{amp}} & \text{if } \hat{\varepsilon} \le 10^{-3} \\ 100 & \text{otherwise} \end{cases} \tag{3.4}$$

with the reference amplitude $\hat{\varepsilon}_{ref} = 10^{-4}$ and C_{amp} is a material parameter. Equation (3.4) is only valid for the range $5\cdot10^{-5} < \hat{\varepsilon} < 5\cdot10^{-3}$.

The model is restricted to strain amplitudes of $\hat{\varepsilon} < 5\cdot10^{-3}$. For larger amplitudes, the mechanism for plastic straining requires a different calculation approach. The same goes for stress states in vicinity of the yield surface, which could allow even small strain amplitudes to cause progressive failure. For this reason, the FE routine should check whether the yield surface is encountered. If so, equation (3.2) cannot be used.

($\hat{\varepsilon} = \|\mathsf{A}_\varepsilon\|$)

AVERAGE STRESS AND VOID RATIO: f_Y, f_p AND f_e

The accumulation rate is influenced by the average stress ratio $\hat{\boldsymbol{\sigma}}^{av} = \boldsymbol{\sigma}^{av}/\mathrm{tr}(\boldsymbol{\sigma}^{av})$, the average mean stress p^{av} and the void ratio e, each with their separate function. The influence of average

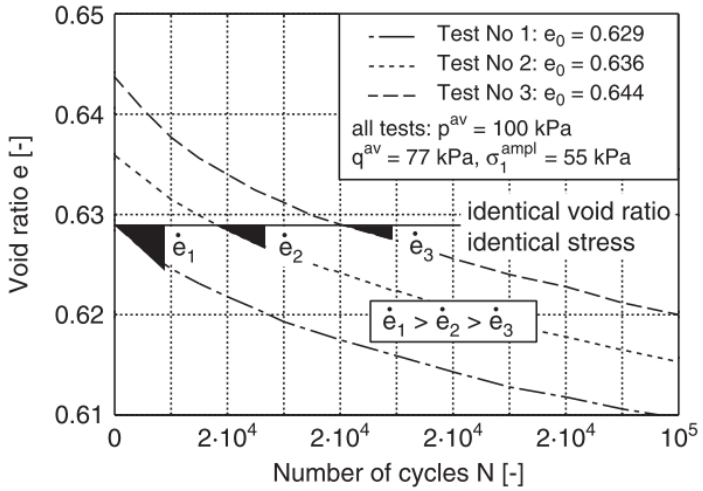

Figure 3.2: The effect of cyclic loading history on the rate of densification $\dot{e}$ =de/dN measured during cyclic drained triaxial tests [1].

stress ratio is approximated by

$$f_Y = \exp\left(C_Y \bar{Y}\right) \tag{3.5}$$

where C_Y is a material constant.

$$\bar{Y} = \frac{Y-9}{Y_c-9}, \qquad Y = -\frac{I_1 I_2}{I_3}, \quad \text{and} \quad Y_c = \frac{9-\sin^2(\varphi_c)}{1-\sin^2\varphi_c}. \tag{3.6}$$

The critical friction angle is denoted φ_c. The stress invariants I_1, I_2 and I_3 depend on $\hat{\boldsymbol{\sigma}}^{av}$ and are defined in Appendix A. The accumulation rate decreases with p_{av} according to

$$f_p = \exp\left[-C_p\left(\frac{p^{av}}{p_{atm}}-1\right)\right] \tag{3.7}$$

where p_{atm} = 100 kPa and C_p a material constant. This approximation is validated for $50 \le p^{av} \le$ 300 kPa. Loose sands will obviously compact more easily than dense sands. This fact of life has been expressed by

$$f_e = \frac{(C_e-e)^2}{1+e}\frac{1+e_{max}}{(C_e-e_{max})^2} \tag{3.8}$$

where C_e is a material coefficient, related to the minimum void ratio e_{min}, e is the current void ratio and e_{max} is the maximum void ratio [8]. More on the determination of these coefficients and parameters can be found in section 3.3. It can be seen from (3.8) that when sand compacts up to the point $e = C_e$, the accumulation rate will become zero because of $f_e = 0$.

CYCLIC HISTORY: $\dot{f}_N$, g^A

The effect of cyclic preloading is of great importance to the magnitude of $\dot{\boldsymbol{\varepsilon}}^{acc}$. Samples which have the same void ratio and are subject to the same average stress and cyclic deviatoric stress amplitude but a different history of loading have significantly different accumulation rates, as can be seen from the results of triaxial tests [1] displayed in Figure 3.2. Not only the number of historic cycles is of importance, but also the amplitudes of these cycles have an influence to the current densification rate $\dot{e}$. The scalar g^A was introduced to take the aforementioned effect into account. It memorizes the history of cycling, i.e. the number of cycles N and their amplitude $\hat{\varepsilon}$.

The rate of accumulation decreases with N proportionally to

$$\dot{f}_N(N_c) \;=\; C_{N1}\,C_{N2}\,\exp\left(-\frac{g^A(N_c)}{C_{N1}\,f_{amp}}\right) + C_{N1}\,C_{N3} \tag{3.9}$$

where

$$g^A(N_c) = \int_{N=0}^{N_c} f_{amp}(N) \frac{C_{N1} C_{N2}}{1 + C_{N2} N} \mathrm{d}N. \tag{3.10}$$

in which N_c is the current number of cycles, f_{amp} is calculated with (3.4) and C_{N1}, C_{N2} and C_{N3} are soil dependent coefficients.

3.1.2. STIFFNESS TENSOR E

The 4^{th}-order, pressure and void ratio dependent stiffness tensor (or elastic predictor), used in the constitutive equation (3.1) is composed by making use of Hooke's law for isotropic materials and two material and state dependent properties: the bulk modulus K and Poisson's ratio ν. The bulk modulus K accounts for the pressure and void ratio dependent behaviour and is calculated with:

$$K = A_K \frac{(a_K - e)^2}{1 + e} \left(\frac{p}{p_{atm}} \right)^{n_K} p_{atm} \tag{3.11}$$

where e is the average void ratio during the current cycle, $p = -tr(\boldsymbol{\sigma})$ the average mean pressure, p_{atm} the atmospheric (reference) pressure and A_K, a_K and n_K are material constants. The Young's modulus, which is an input for the Hooke stiffness tensor, can be found with the conversion formula

$$E = 3K(1 - 2\nu). \tag{3.12}$$

The hereby produced stiffness tensor **E** is used as an input in Equation (3.1).

3.1.3. PLASTIC STRAIN RATE $\dot{\boldsymbol{\varepsilon}}^{pl}$

The requirement of the plastic strain rate $\dot{\boldsymbol{\varepsilon}}^{pl}$ in the constitutive equation of the HCA model can best be explained by observing the effect of neglecting it. The constitutive equation (3.1) then reduces to:

$$\dot{\boldsymbol{\sigma}} = \mathbf{E} : \left(\dot{\boldsymbol{\varepsilon}} - \dot{\boldsymbol{\varepsilon}}^{acc} \right). \tag{3.13}$$

This equation may well describe a homogeneous case (e.g. a single element test) provided that no soil failure occurs (i.e. the stress state may not violate the Coulomb failure criterion). To see whether this is true, let us consider the case where $\boldsymbol{\varepsilon} = 0$, for which $\dot{\boldsymbol{\sigma}}$ is maximal and proportional to $-\boldsymbol{\varepsilon}^{acc}$. Since $\boldsymbol{\varepsilon}^{acc}$ is proportional to the Modified Cam-Clay flow rule **m**, we can conclude: $\dot{\boldsymbol{\sigma}} \sim -\mathbf{m}$. And since **m** always points outside of the yield surface, the stress state can never leave it, nor the Coulomb failure surface.

However, when more than one element is considered in the calculation and non-homogeneous conditions apply, this analogy may not hold. Especially in the case of neighbouring elements for which the rate of accumulation $\boldsymbol{\varepsilon}^{acc}$ is very different, (3.13) may not suffice. This can be illustrated with an example (from [15]) with nine elements, as shown in Figure 3.3(a). In this example, the displacement of the outer boundaries is prevented and the initial stress condition is isotropic. Due to cyclic loading, the outer eight elements have a rate of strain accumulation not equal to zero: $\boldsymbol{\varepsilon}^{acc} \neq 0$. These elements will contract ($\boldsymbol{\varepsilon} < 0$) due to the isotropic stress state. The element in the middle experiences no strain accumulation: $\boldsymbol{\varepsilon}^{acc} = 0$. This element will have to dilate however ($\boldsymbol{\varepsilon} > 0$), due to the conservation of total area. Equation (3.13) will therefore reduce to $\dot{\boldsymbol{\sigma}} = \mathbf{E} : \boldsymbol{\varepsilon}$, which implies that the stress rate $\dot{\boldsymbol{\sigma}}$ has to be positive (inclined towards tension regime). For large enough strain rates, this might result in the stress state crossing the Coulomb failure surface. Since this situation is physically not possible, but is allowed by equation (3.13), it can be seen that the equation is incomplete.

To prevent the stress state from leaving the admissible range, the plastic straining rate $\boldsymbol{\varepsilon}^{pl}$ is inserted to form Equation (3.1). It maps the stress state back onto the yield surface (which is defined by the Matsuoka & Nakai flow-rule) in case of an inadmissible stress state (see Figure 3.3(b)). This

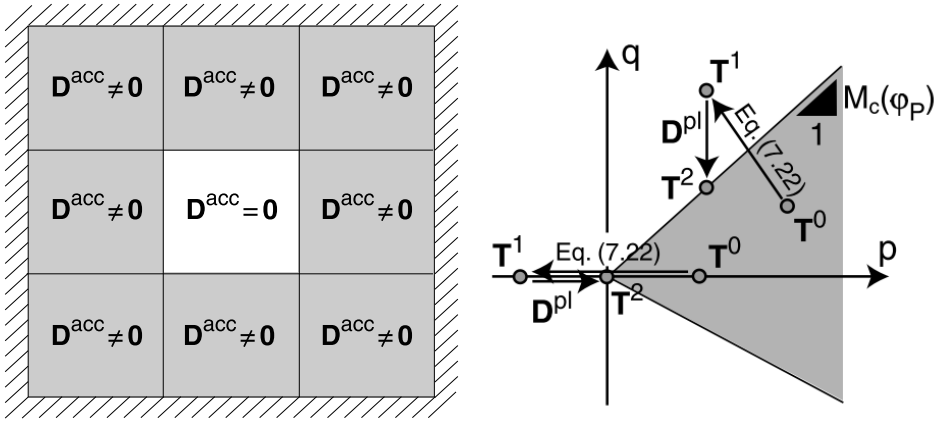

(a) (b)

Figure 3.3: Example which illustrates the requirement of the plastic strain rate $\boldsymbol{\varepsilon}^{pl}$. The strain rate $\dot{\boldsymbol{\varepsilon}}$ is indicated with **D** and the stress rate $\dot{\boldsymbol{\sigma}}$ with **T** in this figure.

is similar to the procedure of elasto-plasticity. The plastic strain rate can also be considered as part of the total strain rate, by replacing the elastic stiffness **E** with the elasto-plastic stiffness tensor in Equation (3.13):

$$\dot{\boldsymbol{\sigma}} = \mathbf{E} : \left(\dot{\boldsymbol{\varepsilon}} - \dot{\boldsymbol{\varepsilon}}^{acc} - \dot{\boldsymbol{\varepsilon}}^{pl} \right) = \mathbf{E}^{ep} : \left(\dot{\boldsymbol{\varepsilon}} - \dot{\boldsymbol{\varepsilon}}^{acc} \right) \tag{3.14}$$

with the elasto-plastic stiffness tensor defined as:

$$\mathbf{E}^{ep} = \mathbf{E} - \frac{\mathbf{E} : \mathbf{m} \otimes \mathbf{m} : \mathbf{E}}{K + \mathbf{m} : \mathbf{E} : \mathbf{m}} \tag{3.15}$$

with **m** the Matsuoka & Nakai flow rule and K the pressure and void ratio dependent bulk modulus. This last approach is applied in the implementation of the model described in chapter 4.

It must be noted that the plastic strain rate is a measure to allow FE implementation, rather than an integral part of the constitutive model.

3.2. PROPERTIES AND COMPLIANCES

3.2.1. COMPLIANCE WITH THE MINER RULE

One limitation of the HCA model is the fundamental assumption that the cyclic strain path in an element of soil is regular and smooth and remains constant over a large number of cycles. This is impractical for many problems when for instance:

- The amplitude and direction of loading is changed frequently.
- The strain loop is a superposition of multiple harmonic oscillations, each with varying amplitudes, polarization and/or frequency of vibration. This could for instance result from either having multiple load sources or an object which vibrates in several of its eigen-modes with corresponding eigen-frequencies.
- The load pattern consist of simultaneous or sequential events of cyclic and monotonic loading.

To overcome this draw-back, effort was made to validate the compliance of the HCA model with the Miner rule. The Miner rule is best known from material fatigue calculations. It dictates that the effect of multiple batches [2] of cyclic loading is independent of the sequence of the batches.

[2] Each load-batch contains multiple load cycles with equal characteristics (amplitude, frequency). The load characteristics only vary between batches.

Therefore, the effects of an irregular load pattern consisting of cycles with (a discrete number of) different amplitudes can be calculated by reorganizing the pattern into blocks of equal amplitude and adding up the effect of each individual block. See Figure 3.4 for a schematic representation of this concept. If the Miner rule is fully valid for the HCA model for all types of load conditions, then the HCA model can be used to calculate many types of geotechnical long-term cyclic loading problems.

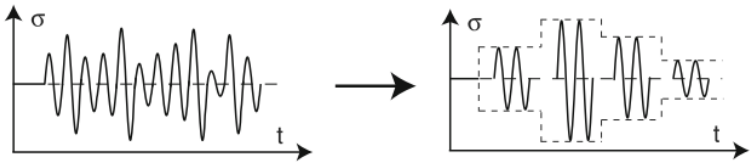

Figure 3.4: Discretization of irregular input to blocks of constant-amplitude cycles. From [2].

The compliance of the HCA model with the Miner rule has been validated in the case of uniaxial loading (triaxial test) on freshly pluviated sand samples [1, 2]. In these tests, the sequence of constant-amplitude load blocks proved to be of negligible influence on the final accumulated strains, see Figure 3.5. However, according to [3], in case of more sophisticated load cases (e.g. multiaxial loading with differences in polarizations or strong ovalities) the results seem to disobey the Miner rule.

One of the cases where the results severely disobey the Miner rule is when the cyclic strain path can be decomposed into multiple harmonic oscillations with different frequencies. In [3] a method for decomposing a strain loop into harmonic functions using a Fourrier spectral analysis is elaborated on. The application of a spectral analysis in combination with the HCA model will require that the behaviour of sand obeys the Miner rule when multiple harmonic loops are applied simultaneously. It is discussed in [3] that in reality this is unfortunately *not the case*. The summation of the results of individual blocks of harmonic vibrations is significantly lower than the result of a single block which is a summation of the same harmonic vibrations (see Figure 3.6). This difference is ought to be the result of the synergy between the harmonic oscillations, which is not taken into account when the strain path is decomposed and calculated separately. It can however be seen from Figure 3.6 that the accumulation as a result from the original complex strain loop can be fairly imitated by analyzing its loop envelope. The tensorial amplitude from the original loop and its envelope ought to be similar. Therefore it can be thought that the current method in the HCA should be able to provide reasonable results, given that the total strain path is considered and not decomposed into its harmonic brick stones.

Another event causing a severe violation to the Miner rule is the case of *cyclic pre-loading*. This is the case when the current average stress ratio ($\eta = q^{av}/p^{av}$) has been higher during a cyclic event in the past. Not only the rate of accumulation is influenced, but also the direction of accumulation changes with respect to the case without cyclic pre-loading [2]. This implies that the modified Cam Clay (MCC) flow-rule provides inaccurate results in such case, since it only takes the current stress state into account (see Figure 3.7). This poses a serious problem for the HCA model because it fundamentally relies on the validity of the MCC flow-rule without exceptions.

3.2.2. CYCLIC STRAIN "MEMORY"

As mentioned in subsection 3.1.1, the parameter g^A was introduced to take the history of cyclic straining into account. This is often referred to by Niemunis and Wichtmann as the cyclic straining "memory" of the soil. Needless to say, the soil does not actually memorize anything, but instead, each load cycle subtly modifies the orientation of the grains and the grain contacts, which increases the resistance of the soil against subsequent load cycles [6]. This process of reorientation of the grains is not fully understood, but there seems to be a consistent relationship between the rate of

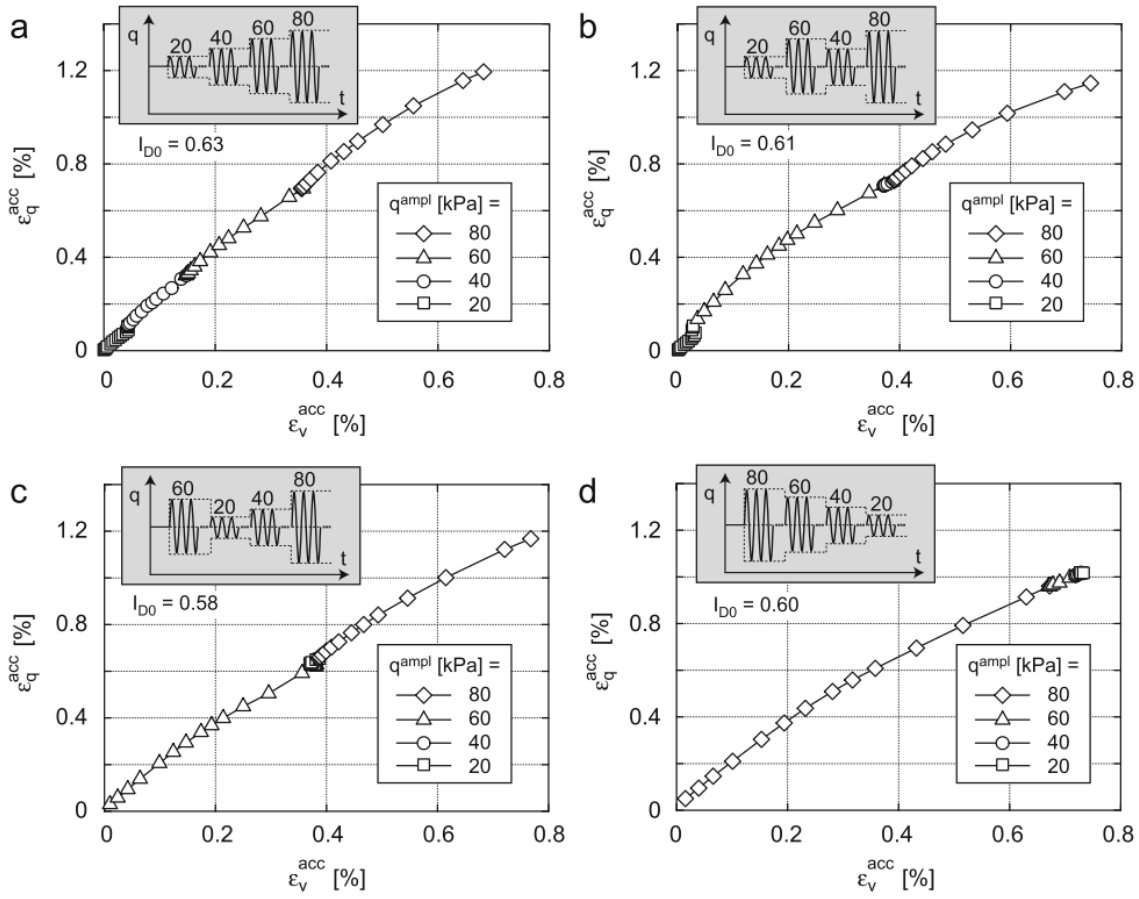

Figure 3.5: Strain paths in four tests where four different equal-amplitude blocks were applied in different sequences, with $p^{av} = 200kPa, \eta^{av} = 0.75, f = 0.25Hz$. From [2].

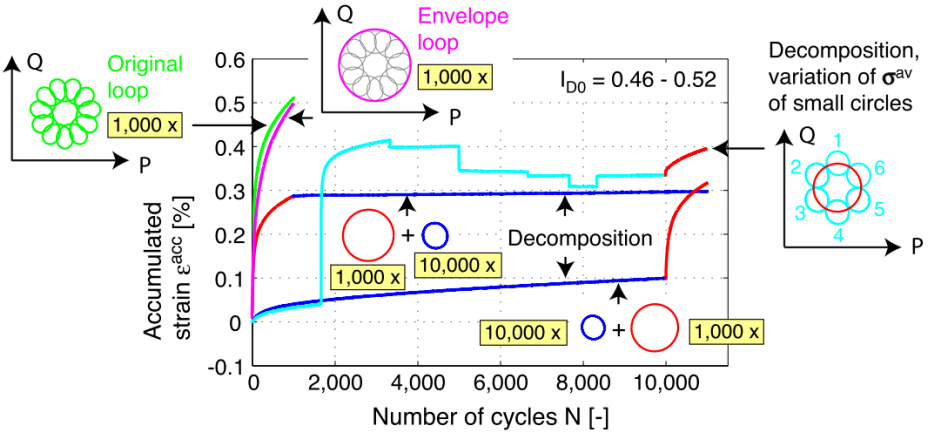

Figure 3.6: Accumulation due to stress cycles consisting two different types of harmonic oscillations [3].

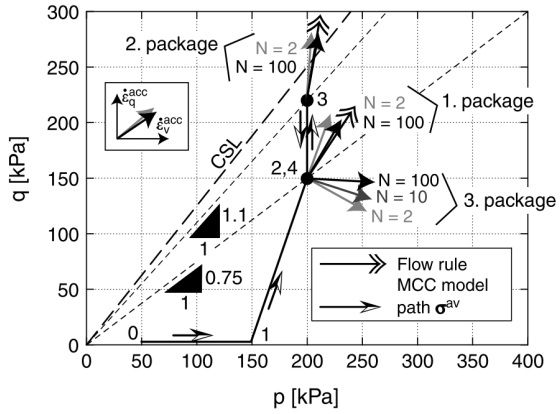

Figure 3.7: Test results from multi-stage cyclic triaxial test with a change in η^{av} between the stages to test the effect of cyclic pre-loading on the direction of straining [4].

accumulation and the amount and magnitude of historic cycles (as if the soil remembers this history). One might ask if it is reasonable that the subtle changes and reorientations of the grain skeleton can be grasped by a single scalar value, representing a "memory" that doesn't really exist. It is admitted by Niemunis & Wichtmann [3] that a scalar might be too simplistic to represent the actual underlying processes correctly and should possibly be complemented with a tensor. However, if the initial condition of the memory can be determined correctly, the method of working with g^A seems to provide reasonable predictions under simple, uniaxial triaxial test conditions.

INITIAL CONDITIONS

Another problem with the memory g^A is that it is not computed based on actual measurements, but by integrating the applied cyclic loading history during a test. This can be done because the initial conditions of the test are known (often freshly pluviated, thus zero cyclic memory). In practical cases where in-field situations are to be evaluated, it is hard - if not impossible - to obtain the current state of cyclic strain memory from in-situ or laboratory tests [3]. Nonetheless, the soils in these cases will most likely not be freshly pluviated and so an initial condition of $g^A = 0$ will most likely overestimate the settlements. However, monotonic loads (i.e. during the construction phase) might make this assumption less unrealistic, as is explained in the next subsection: *Monotonic Preloading*.

For this reason, the authors of the HCA model have proposed a relation between g_A and the liquefaction resistance (see Figure 3.8), which is a measure for the resistance of a soil against liquefaction. As it turns out, this resistance has proven to be a great indicator for the history of cyclic

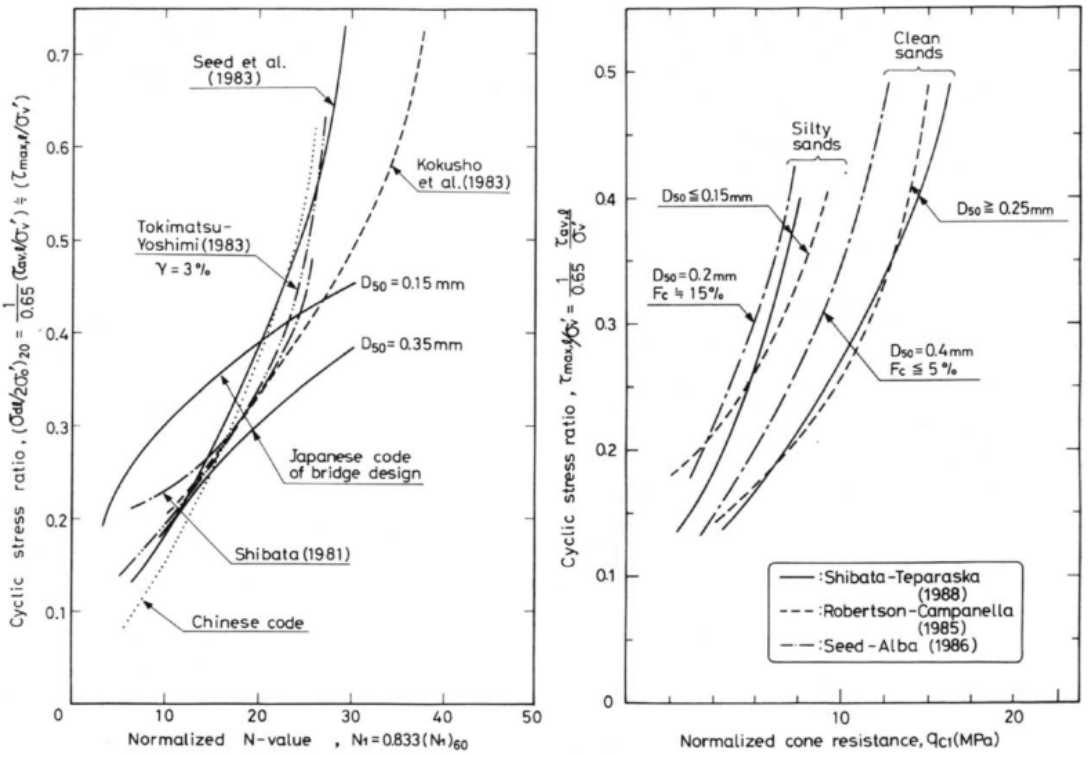

(a) (b)

Figure 3.8: Correlations by various authors for liquefaction resistance based on (a) SPT blow-count and (b) CPT cone resistance [5].

loading [37]. Many correlations can be found by numerous authors between in-situ cone resistance data from CPT tests or blow counts from SPT tests and the liquefaction resistance [5]. The liquefaction resistance of a soil is expressed by the relation between the number of cycles N it would take a cyclic load with a certain cyclic shear-stress ratio ($CSR = \tau^{amp}/p_c$)[3] to cause complete liquefaction of the soil. The normalized parameter $CSR_{N=15}$ defines what the magnitude of the CSR of cyclic loading must be to cause full liquefaction after 15 load cycles. This normalized parameter is used in

$$CSR_{N=15} = CSR_{N=15,0}\, f(g^A) \tag{3.16}$$

where

$$f(g^A) = 1 + C_{g1} \ln\left(1 + C_{g2}\, g^A\right)$$

where C_{g1} and C_{g2} are material constants and $CSR_{N=15,0}$ is the $CSR_{N=15}$ for $g^A = 0$ [5]. A plot of (3.16) together with the data which is was based on can be seen in Figure 3.9

MONOTONIC LOADING

Next to a history of cyclic straining, the soil can also have a history of monotonic (static) loading. It was concluded in [2] that a monotonic preload has no effect on the MCC flow rule and rate of accumulation, as long as all the load cycles occur at the same average stress state. Monotonic preloading could therefore be neglected in the analyses with the HCA model.

However, according to recent discoveries in [6], in case of an increase in average stress (p^{av} or $\eta^{av} = q^{av}/p^{av}$) at the beginning of a new block of cyclic loads, the cyclic memory of the soil is affected. It can be seen in Figure 3.10 that the HCA model severely underestimates the accumulation of strains when subsequent load cycles are preceded by an increase of p^{av} or η^{av}. It can be seen

[3] τ^{amp} = the amplitude of cyclic shear stress; p_c = the effective mean stress.

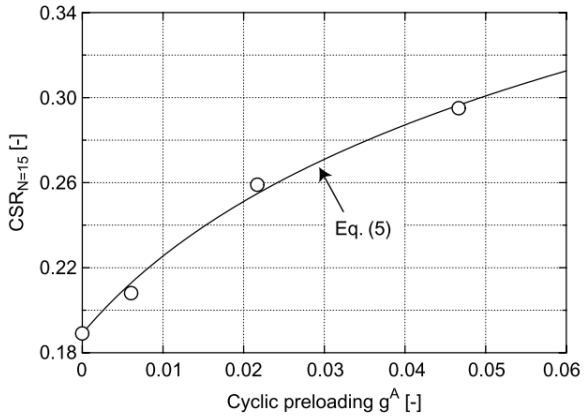

Figure 3.9: Correlation between $CSR_{N=15}$ and g^A for the sand investigated in [5]

from Figure 3.10 that the accumulation paths in such cases can be described effectively by reducing or even resetting the cyclic memory variable g^A to zero after an increase of average stress state. Wichtmann concludes that monotonic strains exceeding 0.4 % will lead to full erasure of the cyclic load memory. More research is required to determine which factors influence the degree of memory loss for the case of strains between 0 - 0.4 % strain, since these results show a large scatter.

The reset of cyclic strain history may prove a useful feature for application of the HCA model at newly constructed structures. The monotonic loads during construction may very well reset the cyclic strain history, leaving the assumption of $g^A = 0$ at $t = 0$ not so unrealistic after all.

3.3. DETERMINATION OF SOIL PARAMETERS

The presented HCA model makes use of quite an extensive set of material constants. Next to the stiffness parameters that are used as input for the stiffness matrix **E** in (**??**), a list of constants $C_\#$ is used throughout the equations in subsection 3.1.1. Also some of the parameters are adopted from the hypoplasticity model, for instance the density limits. These constants and coefficients are described briefly in the following.

3.3.1. HCA COEFFICIENTS

The HCA constants can be obtained by a series of testing methods, which are explained in detail in [2]. In light of practicality, several simple correlations have been proposed between some of these constants and the relatively easily obtained mean grain size d_{50}, uniformity coefficient C_u and minimum void ratio e_{min}. For other constants, no simple correlations have been proposed (yet) and therefore more complex tests should be performed in order to obtain them.

The first simplified correlations have been proposed in [23] for C_{amp}, C_e, C_p, C_Y and C_{N1-3} backed by triaxial test with up to 10^5 cycles on eight clean quartz samples with varying grain size distributions. A new series of tests performed on 14 sand samples resulted in a revision of the correlations [38]. Another revision was made after cyclic triaxial tests with up to $2 \cdot 10^6$ cycles [8], which

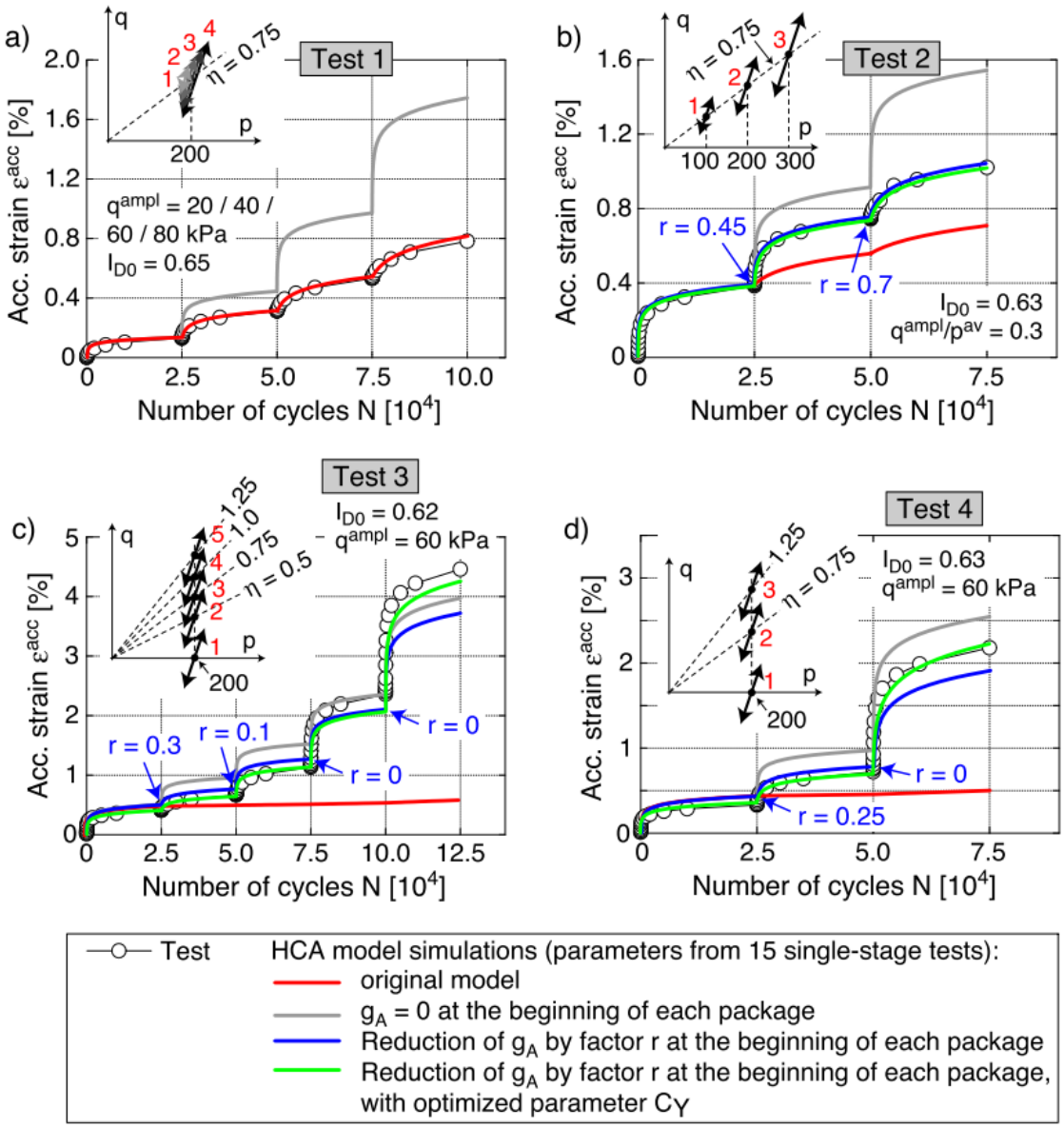

Figure 3.10: Accumulation curves of multi-stage test with applied monotonic loading, calculated by reduced values of g^A [6]

provided the following correlations:

$$C_{amp} = 1.70 \tag{3.17}$$
$$C_e = 0.95 \cdot e_{min} \tag{3.18}$$
$$C_p = 0.41 \cdot [1 - 0.34 \cdot (d_{50} - 0.6)] \tag{3.19}$$
$$C_Y = 2.60 \cdot [1 + 0.12 \cdot \ln(d_{50}/0.6)] \tag{3.20}$$
$$C_{N1} = 0.00184 \cdot [1 - 0.47 \cdot \ln(d_{50})] \cdot (C_u - 1.30) \tag{3.21}$$
$$C_{N2} = 0.00434 \cdot \exp[0.42 \cdot d_{50} + 13.0 \cdot \exp(-0.85 \cdot C_u)] \tag{3.22}$$
$$C_{N3} = 1.83 \cdot 10^{-5} \cdot \exp(-0.37 \cdot d_{50}) \cdot (C_u - 1.23)^{0.59} \tag{3.23}$$

These equations have been validated for quartz sand with mean grain sizes in the range 0.2 mm≤ $d_{50} \leq 3.5$ mm and uniformity coefficients $1.5 \leq C_u \leq 8$. It must also be noted that although the parameters C_{N1-3} have been calibrated for the tests with $2 \cdot 10^6$ cycles, the authors of [8] mention no revision of the other four, hence they are still based on the results of 10^5 cycle tests. The grain size distribution parameters d_{50} and C_u and the densest state e_{min} were obtained with standard methods according to the German DIN code, see subsection 3.3.2. It can be concluded that since C_e (which accounts for the densest possible state in (3.8)) is chosen smaller than e_{min} it was recognized by the authors that the DIN method provides a high boundary for e_{min} values. $C_{\pi 1}$ and $C_{\pi 2}$ can be found for instance with a multi-axial direct simple shear device (DSS). Only several hundred cycles will have to be performed and the loading should have a sudden shift of polarization ($\alpha = 90°$) somewhere half-way. See [1] or [2] for a more detailed description of the procedure. The method of determination of constants C_{g1} and C_{g2} is unfortunately not described well in any of the current literature other than that they should make (3.16) fit the data plot in Figure 3.9. This element of the model is still in a premature stage and needs further research to give more confident correlations. More on the determination of data plots like Figure 3.9 can be found in [5].

The simplified determination of the coefficients of the HCA model by adoptation of equations (3.17)-(3.23) has made the model more convenient to use for practical applications. However, it was noticed by Solf (2011) [39] that in some cases, the adoption of this simplified procedure can result in an overestimation of accumulated strains. She used both the method with extensive tests and the simplified equations to determine the coefficients of the model and reported that the simplified procedure could lead to accumulated settlements of a factor 2 higher than when extensive tests were used.

3.3.2. DENSITY LIMITS

The parameter e_{min} enters the HCA model [1] via the computation of C_e. It should take into account the fact that the sand cannot be compacted any further once its densest state is reached. Sand is at its densest state when the minimum void ratio e_{min} or maximum unit weight γ_{max} is reached. It can also be referred to as a state where the relative density $DR = \frac{e_{max} - e}{e_{max} - e_{min}} = 1.0$.

The authors of [1] have used the methods described in the German standard DIN (1996) [40] for determination of e_{min} and e_{max} of the samples used in the cyclic tests performed to validate their model. It can be seen by the correction factor in equation (3.18) that the obtained value for e_{min} was considered a high boundary value by the authors. Even though this correction was used, still the authors recognize that the model can predict relative densities of $D_R > 1.0$. From a physical point of view this should not be possible.

For the determination of e_{min}, the DIN (1996) standard prescribes the use of a two-prong compaction method. In this method, the sample is saturated and compacted by means of sideways impact hammering[40]. Other National and International standards prescribe different methods for determining this parameter. Variations in compaction type (e.g. vibration, hammering, side-impact), sample state (wet/dry), sample weight requirements and fine contents allowance could

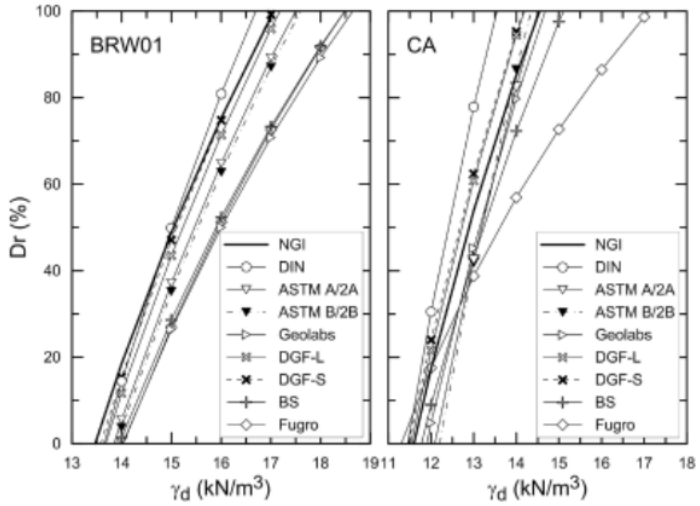

Figure 3.11: Scatter in obtained values of unit weight using various standard test methods for two of the sands investigated. From [7].

result in non-conformities between the same parameters obtained by different methods.

This hypothesis was confirmed by the research by Blaker et al (2015) [7]. Ten different standard methods (including ASTM, BSI, DGF, DIN, Fugro, Geolabs and BGI methods) for determination of γ_{min} and γ_{max} were investigated and compared by testing on five different sands. They found a large scatter in test results obtained by the different methods, especially regarding the γ_{max} (i.e. e_{min}) calculation. Most importantly, it was shown that the DIN (1996) method generally provided the lowest values of maximum unit weight (i.e. highest values of e_{min}) with respect to the other methods. The authors of [7] pose that the difference in maximum density methods could be explained by the differences in applied compaction energy. The methods were also tested for the occurrence of grain-crushing. It appeared that the DIN method was the only method where definitely no grain-crushing occurred, which could also explain the low values of unit weight observed. In Figure 3.11 the scatter in densities found with multiple methods can be seen for two types of sand.

In the tests performed by the authors of [1],[23],[8] and [38], multiple cyclic triaxial tests were performed with up to two million load cycles per test. One could regard such a test as a very extensive compaction test to determine the maximum density of a sample. It can be seen from the tests on well graded sand samples (Figure 3.12) that the accumulated strains tend towards a certain maximum value. An obvious explanation is that this maximum value represents the densest state of compaction and therefore the sand simply cannot compact any further. Sadly, none of the samples have actually reached this maximum value so no definite conclusions can be drawn from this, but the concept of a maximum value of accumulated strain is also recognized by the authors of the tests. It is also recognized that the current HCA model does not predict the curve which indicates a decrease of settlement rate after $\pm 5 \cdot 10^5$ cycles. Therefore, the predicted settlements after two million cycles are an overestimation of the test results for all the tests in Figure 3.12.

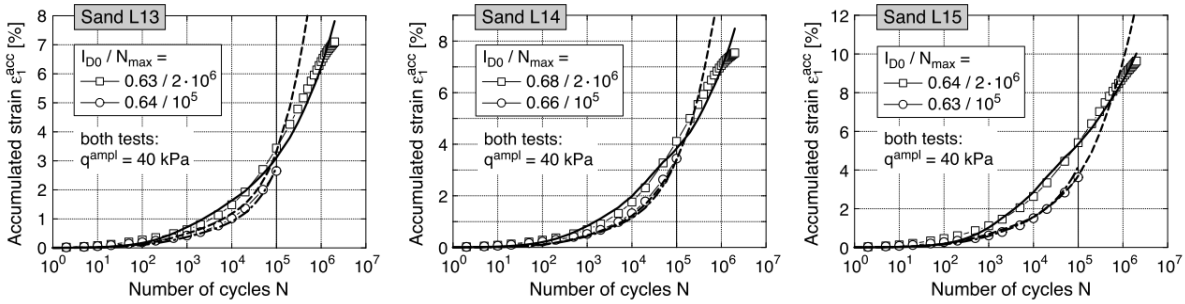

Figure 3.12: Plots of HCA model predictions (lines) and test data (points) for three sand samples loaded up to 10^5 and $2 \cdot 10^6$ cycles. From [8]

3.4. APPLICATIONS

In the recent past, several practical applications of the HCA model have been documented in scientific articles. These applications are to be seen as a proof of concept, as most of the described results have not been validated by data from measurements. A number of these cases shall be discussed in this section to state the lessons learned about the possibilities and limitations of the HCA model. These cases include the estimation of accumulated deformations at:

- A centrifuge model test of a shallow foundation [1].
- Offshore wind power plant (OWPP) foundations in the North Sea [41].
- Dynamic equipment foundations: a gas turbine in granular soil [42].
- The foundation of the 'Deltawerken' at The Oosterscheldekering in The Netherlands [39].
- Pavemens subject to cyclic loading [43].

SHALLOW FOUNDATION CENTRIFUGE TEST

In Niemunis et al. (2005) [1] and Wichtmann et al. (2005) [15], the results of the HCA model for a shallow stip foundation were validated by comparing the calculated settlement with the results of a centrifuge test, which was carried out earlier by Helm et al. [44]. A dry, freshly pluviated sand was used in the centrifuge test, where an increased gravity of 30g was applied. The vertical load on the foundation was chosen as Q^{av} = 88.7 kN, Q^{ampl} = 75.1 kN with a frequency of 0.44 Hz. The 2D FE setup and the comparison of results can be seen in Figure 6.1. The FE calculations were carried out with the FE program Abaqus, where an UMAT routine containing both the Hypoplasticity and HCA models was implemented. It can be seen that the final settlement of the foundation after 10^5 load cycles in the centrifuge test was predicted quite accurately by the FE calculation with the HCA model.

OWPP FOUNDATION

Wichtmann et al. (2011) [41] have used the HCA model to calculate the permanent deformations at Offshore wind power plant (OWPP) foundations in the North Sea. In the paper, a 3D FE calculation in Abaqus was set up, representing a monopile foundation which was unidirectionally loaded with two cyclic load functions. The two load functions represented the overturning moment and the horizontal load, which both contained a constant and (harmonically) time dependent part. The harmonic load functions were of equal frequency and phase during the loading of 10^6 cycles in the FE calculation.

The HCA model predicted the horizontal displacement of the monopile as a function of depth for a range of magnitudes of the average overtuning moment and the amplitude. The results were in compliance with the expectations of the authors, however no validation of results was made. The papers states that a quantitative verification is planned for the future.

DYNAMIC EQUIPMENT FOUNDATIONS

Galindo et al. (2014) [42] used the HCA model in a simplified calculation of the settlements underneath a vibrating gas turbine. The paper not only considers the steady-state mode of operation, but also the transient behaviour during start-up of the turbine. Especially during start-up, the load signal can be very irregular, containing a range of frequencies (0-60 Hz) and strain amplitudes. The problem is strongly simplified, since the authors chose to use a spreadsheet type of calculation instead of using FE software. The soil was spatially discretized as a 1-dimensional problem with horizontal layers of equal thickness. The (elastic) strain amplitudes as a result of each individual load cycle were calculated for each layer, making use of Barkan's equations for dynamic foundation design and assuming a linear decay of strain amplitude with soil depth. Subsequently, the computed strain amplitudes were discretized into threshold groups [4] of 65%, 75% and 90% interval. Each threshold group of equal strain amplitudes was then used as input for subsequent calculations with the HCA model to calculate the final permanent settlements of the gas turbine. The final answers were sensitive to the choice of discretization of the strain amplitudes, but the answers were thought to be conservative since no soil damping was taken into account. It was concluded that the transient (start-up) phase was of greater influence on the total accumulation of permanent strains than the steady-state phase. The results were not validated by comparisson with expermental or in-situ measurements.

PAVEMENTS SUBJECTED TO CYCLIC LOADING

The HCA model was used by Wichtmann et al. (2010) [45] to investigate the permanent deformation of pavements due to the exposure to small cyclic strains over the course of several years. Instead of sand, the applicability of the model on unbound granular material (UGM), used in pavement foundation engineering, was investigated. It was concluded that after the recalibration of several factors and constants, the HCA model provided good predictions of the experimental data from laboratory tests. This proves that the HCA model has potential value for granular materials other than sand.

3.5. THE HYPOPLASTICITY MODEL WITH INTERGRANULAR STRAINS

In section 3.1 it was mentioned that a "conventional model where small strain non-linearity is accounted for" should be used for the implicit phase of the calculation. The hypoplasticity model is an advanced soil model which fits this description. It is also the model of choice in all of the scientific publications on FE implementation of the HCA model available to this date. Therefore, the same version of the hypoplasticity model as used in these publications was used in the FE implementation in this thesis. The model shall be elaborated on in the course of this section.

3.5.1. OVERVIEW

The hypoplasticity model is a non-linear constitutive soil model. It is well described in many publications, e.g. [10, 46–50]. As opposed to known practices at other advanced (elasto-plastic) constitutive soil models, no distinction is made between the elastic and the plastic part of deformations, and therefore the model does not work with the conventional notions of a yield surface or plastic potential surface. It was developed at the University of Karlsruhe (KIT, Germany) during the 1990's. Various versions of the hypoplasticity model have been proposed in the past by Kolymbas (1985), Gudehus (1996), Bauer (1996), Wolffersdorff (1996) and Niemunis & Herle (1997). Initially, only monotonic loads on cohesionless soils could be modelled, but nowadays, also visco-hypoplasticity

[4] For instance, in case of 65% threshold groups, the first group contains N_1 strain amplitudes exceeding 0.65 times the calculated maximum strain amplitude. These amplitudes were then all assumed to have the same (maximum) value $\hat{\varepsilon}_1$. The next group contains the N_2 amplitudes between 0.65^2 and 0.65 times the maximum strain amplitude and were assumed to have the value $\hat{\varepsilon}_2$ of 0.65 times the maximum value. This discretization continues until all strain amplitudes are categorized into a group.

versions are available to model clay as well as sand. In this thesis, only the version for granular materials shall be discussed.

The hypoplasticity model considers the changes in stress in a grain skeleton, due to the rearrangement of the grains. It is based on a few basic assumptions about the grain skeleton [10]:

1. The state is defined only by the grain stress tensor $\boldsymbol{\sigma}$ and density (void ratio e).

2. The grains are permanent, i.e. there is no abrasion and grain fracturing.

3. There is an upper (e_i) and a lower limit (e_d) of the void ratio – macro pores are not allowed for – depending on the effective mean pressure $p' = -\mathrm{tr}\boldsymbol{\sigma}'/3$. The same holds for the critical void ratio e_c, which is reached after large monotonic shearing.

4. Independently from the initial state, proportional deformation paths lead asymptotically to proportional stress paths.

5. The mechanical behaviour of the grain skeleton is rate-independent and the principal of effective stress holds.

6. Cementation and attractive/repulsive forces of the grain contacts are negligible.

The von Wolffersdorff version of the hypoplasticity model [47] is considered to be the current standard version, which includes the Matsuoka-Nakai critical state concept and a stress and density related stiffness matrix. The constitutive model with these concepts are discussed in subsection 3.5.2. To address the problem of ratcheting during cyclic loading, Niemunis & Herle [48] proposed the 'intergranular strain' concept as an extension on the Wolffersdorff hypoplasticity model. This extension is discussed in subsection 3.5.4.

3.5.2. CONSTITUTIVE MODEL AND PARAMETERS

The constitutive equation of the von Wolffersdorff model reads:

$$\mathring{\boldsymbol{\sigma}} = f_e f_b \left[\mathbf{L}\left(\hat{\boldsymbol{\sigma}}, \boldsymbol{\varepsilon}, \varphi_c\right) + f_d \mathbf{N}(\hat{\boldsymbol{\sigma}}) \| \boldsymbol{\varepsilon} \|\right], \tag{3.24}$$

where $\mathring{\boldsymbol{\sigma}}$ is the objective (Jaumann) stress rate and $\mathbf{L}$ and $\hat{\boldsymbol{\sigma}}$ are tensorial parts which depend on Euler's stretching tensor $\boldsymbol{\varepsilon}$, the stress ratio tensor $\hat{\boldsymbol{\sigma}} = \frac{\boldsymbol{\sigma}}{tr\,\boldsymbol{\sigma}}$ and the critical state friction angle φ_c. The scalar factors f_e, f_b and f_d express the influence of stress state and density.

The hypoplasticity model knows a version for granular materials and one for clays (viscohypoplasticity). In the light of the focus of this thesis, only the granular version shall be discussed. The version for granular materials has eight material parameters: φ_c, h_s, n, e_{d0}, e_{c0}, e_{i0}, α and β, which shall be discussed briefly in the following.

The critical state friction angle φ_c determines the resistance of a granulate subjected to monotonic shearing in critical state. In this state, further shearing of the soil will not lead to a change of stress state or volumetric shearing.

The void ratio is a very important state parameter in the hypoplastic model. With an increment of straining, the increment of void ratio is calculated with:

$$\mathring{e} = (1 + e)\, tr\, \boldsymbol{\varepsilon} \tag{3.25}$$

The scalar factors f_d, f_e and f_b depend on the current void ratio e and the limiting void ratios for maximum density e_d, (theoretical) minimum density e_i and critical state e_c. As these limiting void ratios are pressure dependent (see Figure 3.13), they are expressed by the current average stress

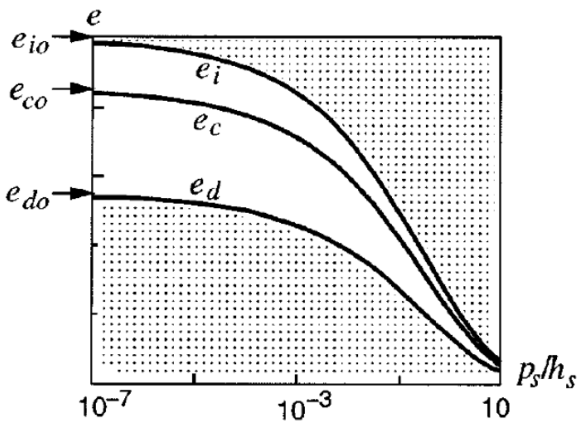

Figure 3.13: The dependency of the reference void ratios on the main stress [9]

$p' = -tr\,\boldsymbol{\sigma}$ and the limiting values at vanishing pressure e_{d0}, e_{c0} and e_{i0}:

$$\frac{e_d}{e_{d0}} = \frac{e_c}{e_{c0}} = \frac{e_i}{e_{i0}} = \exp\left[-\left(\frac{3\cdot p'}{h_s}\right)^n\right] \tag{3.26}$$

The granular hardness h_s and exponent n in this expression determine the shape of the deformation curve in case of isotropic compression, as can be seen in Figure 3.14. The values for critical and

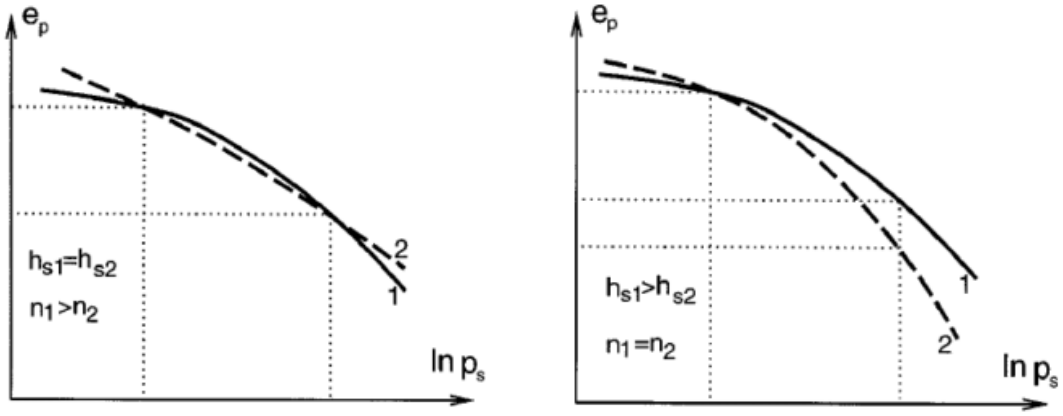

(a) (b)

Figure 3.14: Influence of n (a) and h_s (b) on oedometric curves [9].

maximum density at zero pressure can be determined by standard index tests: $e_{d0} = e_{max}$, $e_{c0} = e_{min}$. $e_{i0} \approx 1.15 e_{c0}$ and $e_{d0} \approx 0.6 e_{c0}$ are widely accepted simple estimates [10].

The pycnotropy factor f_d in (3.24) is determined by the current and limiting states of the void ratio and by the material parameter α. f_d is defined by

$$f_d = \left(\frac{e - e_d}{e_c - e_d}\right)^{\alpha} \tag{3.27}$$

and it controls the transition to the critical state, the peak friction angle and the dilative behaviour of the soil.[5]. The influence of the void ratio on the incremental stiffness is determined by the density factor f_e, defined by

$$f_e = \left(\frac{e_c}{e}\right)^{\beta} \tag{3.28}$$

[5]A modification to the parameter f_d was posed by Niemunis [51], as described in Appendix B.

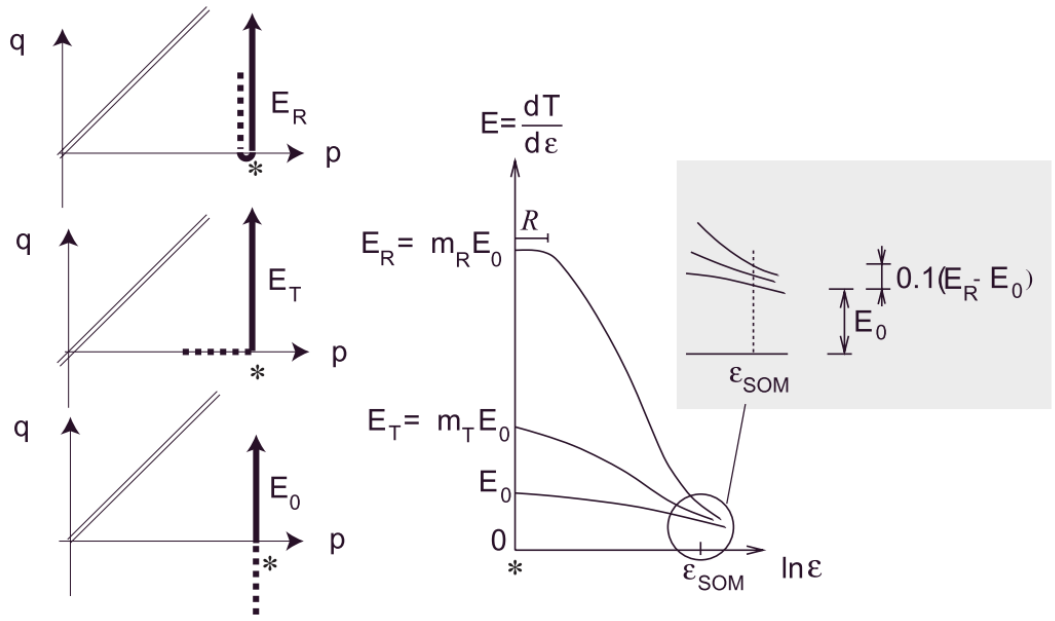

Figure 3.15: Increase of incremental stiffness due to change in the direction of straining [10].

with the material parameter β. The baroptic factor f_b takes into account the increase of stiffness due to an increase of mean stress. It knows a rather elaborate definition, which can be schematized as:

$$f_b = f\left(p', e, e_{i0}, e_{c0}, e_{d0}, \alpha, \beta, h_s, n, \varphi_c\right) \tag{3.29}$$

3.5.3. INCREASED SHEAR STIFFNESS MODIFICATION

It is discussed in [49] that the shear stiffness in the original hypoplasticity model described above is too low for low stress paths with a relatively low shear stress amplitude. Therefore, a modification of the formula for **L** and **N** was drawn by Niemunis, as described in Appendix B, [49] and [15].

3.5.4. INTERGRANULAR STRAIN EXTENSION

The intergranular strain concept is used as an extension on the original von Wolffersdorff hypoplasticity model to better predict the soil behaviour for small strains. It takes into account the temporal increase in material stiffness due to a change in direction of straining. The increase is governed by the direction of straining $\boldsymbol{\varepsilon}$ and the intergranular strain tensor $\boldsymbol{\delta}$, which stores the most recent direction of straining. The inter granular stain extension requires five additional material parameters: m_T, m_R, R, β_R and χ. The factors m_T and m_R determine the amount of stiffness increase right after the change of strain direction, whereas a 90° rotation in strain direction leads to $E_T = m_T \cdot E_0$ and a 180° rotation leads to $E_R = m_R \cdot E_0$. Furthermore, R controls the elastic strain range and the two exponents β_R and χ control the decay of the stiffness increase after a change of strain direction. A visualisation of how the strain path and the mentioned factors influence the incremental stiffness can be seen in Figure 3.15.

3.6. SUMMARY & DISCUSSION

The HCA model by Niemunis et al. [1] was explained in the course of this chapter. It can be used to calculate the accumulation of plastic strains and stress relaxations in granular materials due a high number of strain cycles ($N > 1 \cdot 10^5$) with a relatively low cyclic strain amplitude ($\boldsymbol{\varepsilon}^{ampl} < 1 \cdot 10^{-3}$). The constitutive equation of the model allows an explicit calculation method in FE calculation,

which has the potential to increase the accuracy of the results for a large number of cycles, while also drastically decreasing the required runtime of calculations. The explicit calculation of the accumulation rate $\boldsymbol{\varepsilon}^{acc}$ is made possible by assuming that the rate of accumulation is solely dependent on a number of material properties and boundary conditions, including (but not limited to) the amplitude of cyclic straining $\boldsymbol{\varepsilon}^{ampl}$, the stress invariants and the history of cyclic straining. These assumptions have been validated with the results of a number of cyclic triaxial tests with medium dense sand samples which were subjected to up to two million load cycles with variations in amplitudes, average stress levels and initial densities.

In FE calculations, the strain amplitude $\boldsymbol{\varepsilon}^{ampl}$ can be calculated in a preceding calculation phase with another soil model which can account for the increased small strain stiffness of sand and can accurately predict cyclic loading behaviour of sand. For this aid, the authors of the model have continuously used the hypoplasticity model with intergranular strain extension and increased shear stiffness modification in their publications.

For the case of irregular load functions, the validity of the model is heavily dependent on its compliance with the Miner rule. The Miner rule dictates that for irregular load signals, sequencing is of no importance to the final result. This rule has been validated for load signals on sand with irregular variations in amplitude, but constant frequency and average stress. The rule allows a rearrangement of an irregular load signal into a signal with batches of constant amplitude which can be calculated subsequently with the HCA model. It has to be noted that, since the sequence of loading is altered, time-dependent effects – such as the development of excess pore water pressures in time – cannot be taken into account correctly with this method.

A draw-back of the model is that sand does not seem to behave in compliance with the Miner rule when multi-frequency effects are taken into account. The super-positioning principle does not apply for the effects of a load function which consists of multiple harmonic functions with different frequencies. As a consequence, frequency analysis using a Fourier transform cannot be used as a way to generate the input batches for the HCA model. Therefore, the HCA model can solely be used if it is justified to represent the load signal as a harmonic function with a single frequency. This is can be a major draw-back for problems with multiple load sources, or structures which vibrate in multiple eigen-frequencies.

The HCA model also seems to provide unrealistic results when cyclic loading is combined with monotonic straining. Monotonic strains can erase the effects of the history of cyclic loading, which will increase the rate of accumulation. Although this effect might provide a solution to another problem – concerning the assessment of the initial conditions of cyclic "memory" – no clear relationship has been found between the magnitude of monotonic strains and the degree of cyclic "memory loss".

Another case for which the HCA model provides unrealistic results is the case of cyclic preloading. It undermines the validity of the intrinsic assumption of the model that the direction of straining is solely dependent on the stress state.

The HCA model requires 12 material parameters that should be determined with a series of laboratory tests. Also an initial value for the cyclic strain "memory" should be provided. If the model is used in combination with the hypoplasticity model with intergranular strain, another 13 material parameters and 4 initial state parameters should be determined. The determination of all these parameters can be quite laborious. A simplified method to assess seven of the HCA material parameters was proposed in literature, but was also observed to provide inaccurate results.

Concluding, the HCA model can be a useful tool to assess the accumulation of strains and stresses for boundary value problems that involve long-term cyclic loading. However, since the HCA model has some strict limitations to the applicable range of load scenarios, caution should be taken before application of the model.

4
FE IMPLEMENTATION

The constitutive equation of the HCA model (which is discussed in section 3.1) can be implemented into commercially available finite element (FE) software. An implementation for the FE program Abaqus was made by the author of the model, as stated in [1]. A recent version of this routine was provided to the author of this thesis. Both Abaqus and Plaxis can accept user defined material models: models which are not present in the standard model library of the FE software. They should be manually programmed with a programming language such as Fortran and compiled into a dynamic link library (DLL) file. Upon startup, the software loads the models present in the DLL file and thereby temporarily adding them to its library of models. The FE software expects certain routines to be present in the model, such as formulas for the calculation of stress and stiffness tensors.

Abaqus can be used for FE analyses for a broad band of engineering problems. The wide variety of applications makes the software very versatile, but also reduces the user-friendliness due to the large number of parameters and model settings of which the user is required to be knowledgeable. This is in great contrast to the FE software Plaxis, which is less versatile since it can only be applied to geotechnical engineering problems, but is on the other hand very user friendly.

The majority of engineering companies in the Netherlands that deal with geotechnical problems are well acquainted with Plaxis. Implementing the HCA constitutive model in Plaxis would therefore make the model available to a large group of end-users. The source code for the HCA model implementation in Abaqus was used as a starting point for this aid. Along with the HCA code, also a version was provided of the von Wolffersdorff hypoplasticity model with two extensions: intergranular strain and adjustable Poisson's ratio. This model was also implemented in Plaxis with the aim to calculate the first two cycles of loading.

In the course of section 4.1, the differences between the user defined routines in Abaqus and Plaxis are discussed and compared with the aim to give insight in the method of converting the compatibility of the HCA code from Abaqus to Plaxis. The specifics of the conversion are discussed thereafter in section 4.2.

4.1. USER DEFINED ROUTINES

Although the FE calculation procedures in both Abaqus and Plaxis are similar, they both expect slightly different elements to be present in the code of the DLL file. For instance, Plaxis carries out the calculation in a specific sequence and expects the DLL file to be structured likewise, whereas Abaqus does not expect such a structure. Furthermore, most deviations originate from alternative use of syntax, i.e. the parameters and routines have different names. One might say that both programmes carry out quite similar work, but speak a different dialect.

Examples are known where a DLL file originally written for Abaqus was made available for calculation in Plaxis by means of writing a 'wrapper'. This can be seen as a code which translates between the two languages of the software programs. The advantage of this approach is that, in principle, the original code can be left unaltered, which minimized the chance of severe bugs due to erroneously rewriting of the code. The differences between the routines in Abaqus and Plaxis concerning user defined modelling are discussed in the course of this section.

ID Task	Expected action
1	Initialize state variables *StVar0*
2	Calculate stresses
3	Calculate effective material stiffness tensor
4	Initialize number of state variables
5	Define stiffness tensor options
6	Calculate elastic material stiffness tensor

Table 4.1: Cases of IDTask argument for Plaxis UDSM.

In the rest of this report the abbreviations 'UMAT' and 'UDSM' shall be used. They stand for the names Plaxis and Abaqus have given to their routines for manually implemented user-created material models. Plaxis uses UDSM, which stands for 'User Defined Soil Model', while Abaqus uses UMAT, which is short for 'User MATerial model'.

ABAQUS UMAT

The DLL file for a UMAT routine is written in the Fortran '77 programming language. The code starts by proclaiming the name of the routine and its arguments, as stated below. Some of the most utilized arguments are described in Table C.1. More detailed information about writing Abaqus UMAT routines can be found in the Abaqus UMAT lecture [52].

```
SUBROUTINE HCA_UMAT (stress,statev,ddsdde,sse,spd,scd,rpl,ddsddt,drplde,
drpldt,stran,dstran,time,dtime,temp,dtemp,predef,
dpred,cmname,ndi,nshr,ntens,nstatv,props,nprops,
coords,drot,pnewdt,celent,dfgrd0,dfgrd1,noel,npt,
layer,kspt,kstep,kinc)
```

PLAXIS UDSM

The UDSM subroutine should be named USER_MOD and is called with the syntax below. The most important arguments of the subroutine are described in Table C.2. For a more detailed description of the use of Plaxis UDSM, reference is made to th Plaxis material models manual [53].

Plaxis calls the UDSM routine for specific information. For instance, during initialization of the model it will want to retrieve the number of state variables only. The type of information or calculation which it expects during a subroutine call is indicated by the argument *IDTask*, which can have integer values between 1 and 6. An overview of expected actions and corresponding values of *IDTask* can be seen in Table 4.1. The sequence of *IDTask* calls is conveniently chosen by Plaxis: 4, 5, 1, 3, 2, 6. Task 4, 5 and 1 are only executed at the initialization of the calculation phase. Tasks 3, 2 and 6 are executed during every step for each integration point. Steps 2 and 3 are repeated in every iteration. Another UDSM argument is *iMod*, which is convenient when the USER_MOD subroutine contains multiple soil models. Argument *iMod* obeys the model number which can be selected via the user-interface in the Plaxis input program. The UDSM code should then select the correct number based on the integer value of *iMod* which corresponds to the correct model.

```
Subroutine User_MOD (IDTask,iMod,IsUndr,iStep,iTer,iEl,Int,X,Y,Z,Time0,
dTime,Props,Sig0,Swp0,StVar0,dEps,D,BulkW,Sig,Swp,
StVar,ipl,nStat,NonSym,iStrsDep,iTimeDep,iTang,
iPrjDir,iPrjLen, iAbort)
```

4.1.1. ANALYSIS AND COMPARISON OF UMAT AND UDSM

It can be seen by comparing Tables C.1 and C.2 that a number of arguments in the UMAT and UDSM subroutines differ in name, but carry the same content. For instance, the argument *stress* in UMAT

and *Sig* in UDSM are both utilized to store the Cauchy stress tensor. Next to this, there are also some fundamentally different arguments, like *IDTask* in the UDSM Subroutine. As mentioned before, in both the UMAT and UDSM routines, the argument *props* is used to store the material properties. These properties (such as strength and stiffness properties of the soil) are provided via a user-interface menu FE programs. Also a list of state variables can be stored in both of the routines. State variables are variables that can change during the calculation steps and should therefore be updated in each step to their current state. They are passed on to subsequent phases, as long as the material model remains the same.

It must also be noted that Plaxis and Abaqus have a different way of providing and calculating strain and stress vectors. First of all, in all 6-dimensional tensors related to stress or strain (e.g. the Cauhcy stress tensor) the 5^{th} and 6^{th} entry are interchanged. Furthermore, the UMAT routine receives both the current strain tensor as well as the incremental strain tensor from the Abaqus kernel, while the Plaxis kernel only provides the incremental strain tensor. In Abaqus, the rotation of elements is also taken into account by providing the deformation gradient tensor. A final issue results from a different definition of strain in both programs. The HCA UMAT routine was programmed to receive 'true strain', also known as 'Hencky strain'[1] . Plaxis defines all strain as engineering strain and is not able to calculate true strains directly. A workaround has been introduced with the 'updated mesh' feature, which is not the same thing as calculating true strains, but it comes close. The differences between true strains and engineering strains become evident only for large strains ($\varepsilon > 5\%$).

4.2. CONVERSION OF THE HCA UMAT ROUTINE TO PLAXIS UDSM

The source code for the HCA model was provided by Dr. Andrzej Niemunis in UMAT format. One of the conditions for providing this code was that no part of the code was to be distributed to persons other than the author of this thesis. Therefore, since this thesis is to be made publicly available, the source code can not be discussed in detail. The original code, named 'HCA CUMAT 2010', has been used as a starting point for the implementation in Plaxis. An Intel Fortran compiler (iFort) has been used to compile the source code to two DLL files[2].

4.2.1. STEPS OF CONVERSION

The routine in the source code consists of three modes of operation: 'Initial/monotonic', 'recording' and 'explicit creep'. In the first two modes, a Woldersdorff implementation of the hypoplasticity model with intergranular strains was called to calculate the effects of monotonic and dynamic loading. In the recording mode, an algorithm was used to record the calculated strain loop into the list of state variables. In the 'explicit creep' mode, the HCA model code is called. Instead of making use of a variable like *iMod*, the UMAT routine determines which operation mode should be used by analyzing the phase number.

For implementation into Plaxis, the three modes of operation had to be implemented as three different soil models which are loaded from one DLL file (see 4.1). Initially, the three models have been separated so that each one can be selected by changing the value of *iMod* in the Plaxis Input program. In practice, this is done by selecting the correct model from a drop-down menu. All three models had been programmed to accept the same list of state variables, since the state variables are used as the internal memory throughout all phases of the FE calculation. However, with this method of selecting the different models in the Plaxis Input program, the material model of the soil body has to be changed at multiple times in between the calculation phases. This is not desirable,

[1] The true strain is defined as a derivative of deformation with respect to the current dimensions, whereas engineering strain is defined as the total deformation with respect to the dimensions at the start of deforming. True strain provides a more realistic answer, however is often not so easy to compute. Engineering strains are much easier to compute and only become inaccurate for large strains ($\varepsilon > 5\%$).

[2] In order to run Plaxis 2D in 64 bit mode, both a 32 and 64 bit compiled DLL file need to be present in the Plaxis UDSM folder.

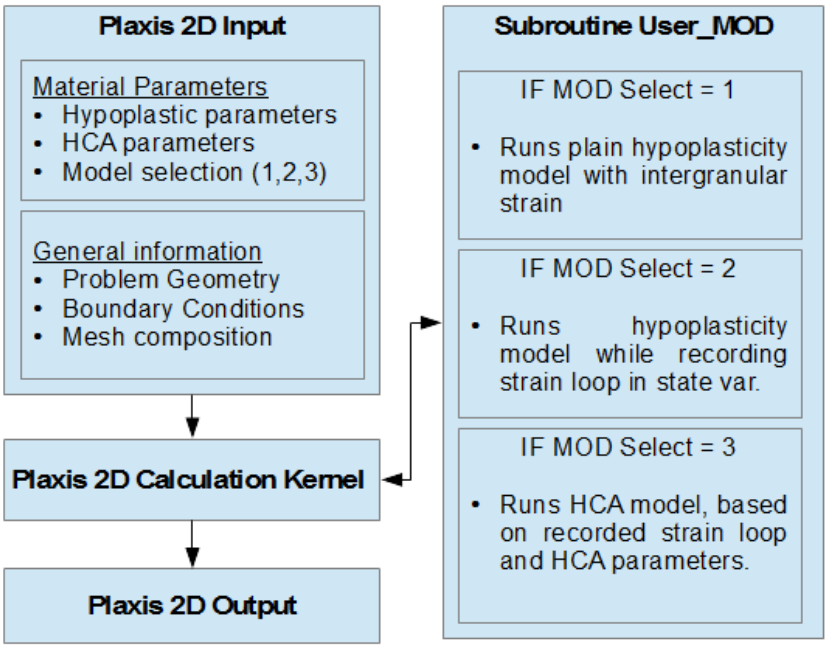

Figure 4.1: Plaxis HCA UDSM internal calculation scheme.

since Plaxis resets the state variables when a new material model is selected. It reckons the information is no longer required, which is true for most soil models. But since the HCA model is somewhat unconventional, some improvisation was required to preserve the memory stored in the state variables. Instead of using *iMod* as the parameter for selecting the model, a new material variable was introduced: *Mod_Select*, which can be assigned a (real) value in the material properties menu and is therefore stored in the *props* argument. This real value is rounded off to the nearest integer value, which can be 1, 2 or 3. With this little trick, *iMod* can be left unchanged, which prevents Plaxis to reset the state variables. At the same time, the material model can indeed be altered by changing the 'material property' *Mod_Select*. An overview of the internal calculation scheme can be seen in Figure 4.1.

WRAPPER

As mentioned before, a wrapper can be coded to simplify the conversion of the UMAT routine. The wrapper acts like a translator between the language of the UMAT and UDSM routine. It converts the variables provided by Plaxis into variables that could be accepted by Abaqus and provides those to the UMAT routine. The UMAT routine can therefore run its original calculation. After completion of the UMAT calculations, the resulting variables are converted back to Plaxis variables, so that they can be interpreted by the Plaxis kernel. A schematic representation of this process is demonstrated in Figure 4.2.

HYPOPLASTICITY MODEL

The HCA code provided by Dr. Andrzej Niemunis also included the von Wolffersdorff implementation of the Hypoplasticity model with intergranular strains and adjustable Poisson's ratio. A wrapper was also written for this model in order to make it compatible with Plaxis. Since the specifics on the implementation of the hypoplasticity model is of less importance to this thesis, it shall not be discussed in further detail.

4.2.2. MATERIAL PROPERTIES

Since both the hypoplasticity model and the HCA model are called within the same UDSM, the material parameters need to be stored into one array. In plaxis, these parameters can be entered into

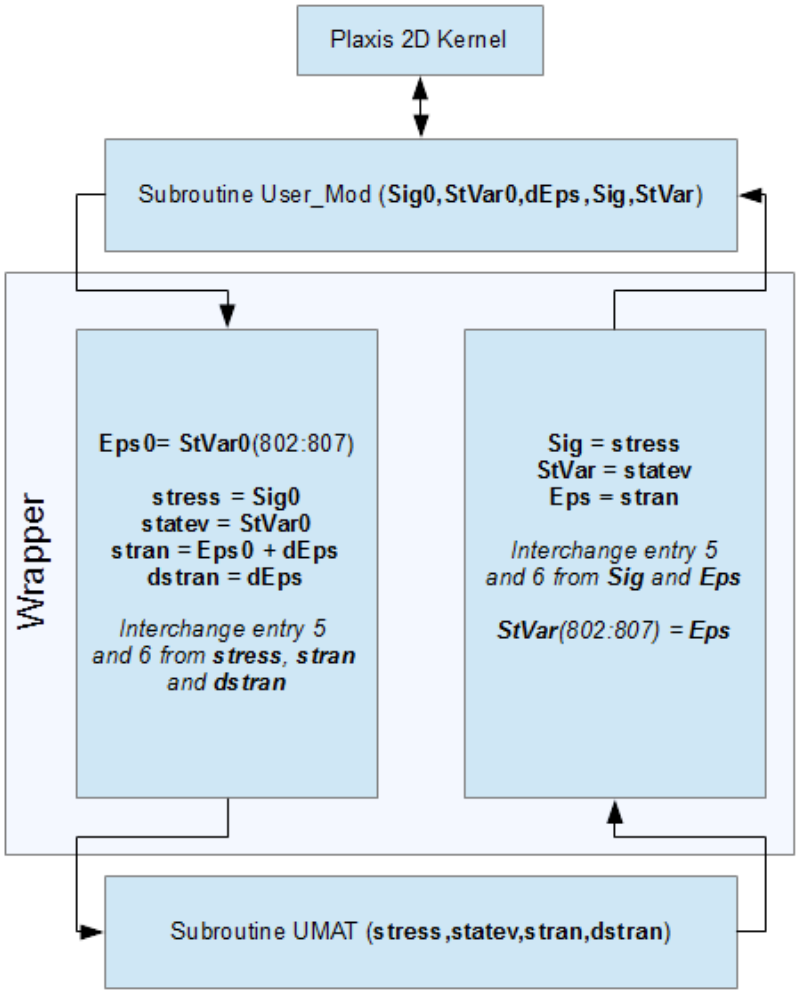

Figure 4.2: Schematic representation of the wrapper function.

the material properties window, see Figure C.1. The total list of properties can be seen in Table C.3.

4.2.3. STATE VARIABLES

The HCA model requires some memory during calculation steps which can be stored and accessed throughout multiple phases of calculation. This memory is stored in the state variables array. The array contains values of function variables such as f_{amp}, the mobilized friction angle φ_{mob} and cyclic strain memory g^A, as can be seen in Table C.4. These entries are mainly implemented for plotting purposes. It also contains some variables for debugging purposes. The majority of entries is part of an array like a vector or tensor. There is for instance the vector of intergranular strain parameters (6 entries), the tensorial amplitude A_ε (81 entries), the back amplitude tensor $\boldsymbol{\pi}$ (81 entries), a stress tensor (9 entries) and the array of recorded points of the strain loop (90 entries). As a result, the array of state variables contains 277 entries. It was confirmed by Plaxis customer support that this unusual high number of entries should not cause any problems in the calculation kernel.

4.3. MODIFICATION TO THE ELASTO-PLASTIC PREDICTOR

The above described transformation of the HCA code to the UDSM format involved no actual adjustments to the inner workings of the model, but merely a rearrangement of the structure and the renaming of some of its elements. However, since the unaltered implementation resulted in problems with numerical convergence (as described in subsection 6.4.1) a slight adjustment was made to the computation of the elasto-plastic predictor.

In order to describe and justify this adjustment properly, first a brief and global overview of the Plaxis 2D stepwise numerical calculation scheme is given in the following subsections.

4.3.1. THE NUMERICAL CALCULATION SCHEME

Every step in the FE calculation starts with information about the initial condition, concerning the location of the nodes in the mesh, the stresses and strains in the integration points and the externally applied load condition. The external forces are stored in the external load vector $\mathbf{f}_{ex}$. It contains the forces in each node, caused by point loads and distributed loads, also including the unit weight of the soil. All the forces depend on the boundary conditions and geometry of the problem alone and therefore, the external load vector is considered to be known and constant during the calculation step. The internal forces (stored in the reaction vector $\mathbf{f}_{in}$) can be found by taking the integral of the stresses in each integration point:

$$\mathbf{f}_{in} = \int \mathbf{B}^T \boldsymbol{\sigma}_c \, dV \tag{4.1}$$

where $\mathbf{B}$ is the strain interpolation matrix[3] and $\boldsymbol{\sigma}_c$ the stress vector computed by the constitutive model. The reaction vector depends on the distribution of stresses, computed by the equations of the constitutive model and is therefore considered to be the unknown vector that is to be solved for. The reaction vector and external load vector should be equal to achieve force equilibrium. A calculation step is started by adjusting the external load vector to the new situation. There is now a discrepancy between the internal load vector at the beginning of the step and the external load vector at the end of the step. This difference is called the unbalance vector:

$$\Delta \mathbf{f}^i = \mathbf{f}^i_{ex} - \mathbf{f}^{i-1}_{in} \tag{4.2}$$

where i is the counter for the current step. The goal of each calculation step is to reduce the unbalance vector to approximately zero. This is achieved by applying finite translations to each node

[3]The strain interpolation matrix $\mathbf{B}$ is the matrix of spatial derivatives of the strain interpolation functions, which describe the continuous transition of strain values in between the discrete values in the nodes.

(with the displacement vector $\Delta\mathbf{v}$), which will result in finite increments of strain and stress in each integration point. The idea is to find the displacement vector $\Delta\mathbf{v}$ that produces a reaction force which is in equilibrium with the externally applied loads.

The displacement vector is searched for by solving the equation

$$\Delta\mathbf{v} = \mathbf{K}^{-1}\Delta\mathbf{f} \tag{4.3}$$

where $\mathbf{K}$ is the global elastic stiffness matrix, which is calculated with the elastic stiffness matrix $\mathbf{E}$ provided by the soil model: $K = \int \mathbf{B}^T\mathbf{E}\mathbf{B}\,dV$. Equation 4.3 provides a prediction of the required node displacements, assuming linear elastic behaviour. In case of linear elastic soil behaviour (i.e. no stress or state dependency of the soil stiffness) the correct displacements should be predicted accurately enough with this routine, provided that the computed stiffness matrix is accurate.

However, in case of non-linear soil behaviour (as is the case in elasto-plastic soil models), the required displacements will be underestimated by the elastic predictor due to the graduate reduction of soil stiffness with increments of strain. To check whether such plasticity effects play a role, the constitutive model is utilized to check whether the displacement vector produces the predicted reaction vector. Since the constitutive equations are expressed in terms of stress and strain, first the displacements in the nodes need to be translated into strains in the integration points with

$$\Delta\boldsymbol{\varepsilon} = \mathbf{B}\Delta\mathbf{v} \tag{4.4}$$

The constitutive model can now calculate the new stress vector, which can be translated to the reaction vector with Equation 4.1. The unbalance force can be calculated with Equation 4.2. If its values are below a certain threshold limit, the step is accepted and the process continues to the next step.

However, in the case of an inaccurate stiffness matrix (which is the case when the elastic stiffness matrix was used to predict plastic behaviour), the resulting unbalance may be larger than the threshold value. The prediction can not be accepted but instead an iterative process is started. The iteration scheme consists of a predictor-corrector scheme and we can consider the previous calculation as the first iteration (iteration counter $j = 1$). The next iteration ($j = 2$) starts with the remaining unbalance vector $\Delta\mathbf{f}^{ij}$ and the stiffness matrix K^{ij} (which may or may not be constant for all iterations). A new displacement prediction is made for the current iteration:

$$\delta\mathbf{v}^{ij} = \left(\mathbf{K}^{ij}\right)^{-1}\Delta\mathbf{f}^{ij} \tag{4.5}$$

where $\delta\mathbf{v}^j$ is the displacement vector for the iteration. The displacement vector for the total step can be found by substitution: $\Delta\mathbf{v} = \Sigma\delta\mathbf{v}^j$. Subsequently, the correction step is applied and the new unbalance is calculated. This process is repeated with new iteration steps until the unbalance is lower than a certain threshold value. Examples of the process can be seen in Figure 4.3.

As mentioned before, the stiffness matrix can be updated at different stages of the process. In a fully linear elastic iteration scheme, the elastic predictor is computed at the beginning of the calculation and used throughout every step and iteration. When non-linearity plays a role and the stiffness matrix is dependent on the current state of stress or density, the stiffness matrix can be updated at the beginning of each step using the modified Newton-Raphson iteration scheme (see Figure 4.3(a)). For faster convergence, the Full Newton-Raphson iteration scheme can be used, in which the (tangential) stiffness matrix is updated with every iteration (see Figure 4.3(b)). This method may however prove less robust (e.g. lead to divergence in the calculation) in case of large fluctuations and local minimum values in soil stiffness.

4.3.2. THE HCA STIFFNESS TENSOR

In the HCA model, a stress and density dependent stiffness tensor is used, as described in subsection 3.1.2. Therefore, the Modified or Full Newton-Raphson iteration scheme can be used. However,

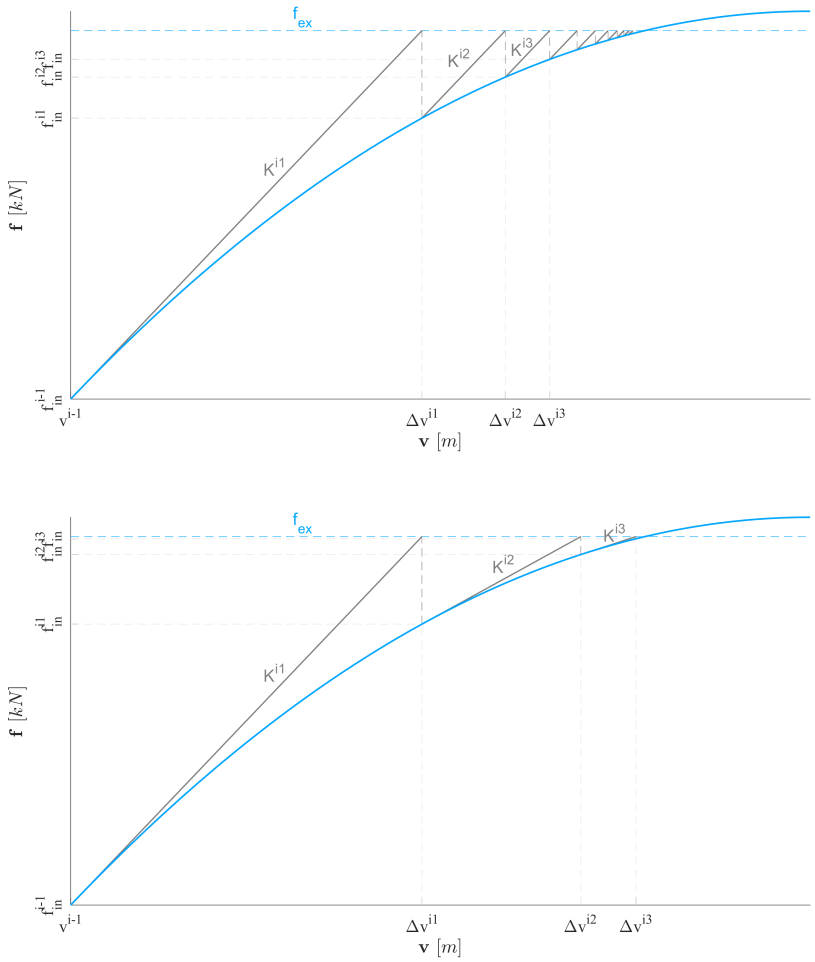

Figure 4.3: Iteration schemes: (a): Modified Newton-Raphson; (b): Full Newton-Raphson.

since not only the stiffness tensor but also the rate of accumulation $\dot{\boldsymbol{\varepsilon}}$ is highly dependent on stress and density parameters, full Newton-Raphson iteration was thought to be prone to numerical instability. Therefore, a modified Newton-Raphson scheme was used.

In the case of severe plasticity effects, the number of iterations required to reach sufficient accuracy may be rather high. A large number of iterations is undesirable since this will increase runtimes drastically. In the HCA model, this may be the case when the stress state is projected onto the Matsuoka-Nakai yield surface. In such case, the elastic predictor is replaced by the elasto-plastic (EP) predictor, as described in subsection 3.1.3. The EP stiffness is lower than the elastic stiffness, which results in a faster rate of convergence. However, if the stiffness is chosen too low, the solution may not converge at all. Such problems were observed during the verification of the model, as described in subsection 6.4.1.

The problem with the EP predictor seems to be that the predicted stiffness may be lower than in reality. This could be caused by a local increase in soil stiffness due to an increase of average stress or density. Especially in zones which are characterized by low stress states and high stress gradients, the decrease of soil stiffness due to plasticity effects might be considerably lower than predicted by the EP predictor. The consequence of this is that the predicted strain increments may exceed the actual strain increments. In such a case, the iteration process cannot converge to the optimal value, but will diverge towards unrealistic values. These effects were observed regardless of the choice of (Newton-Raphson) iteration scheme.

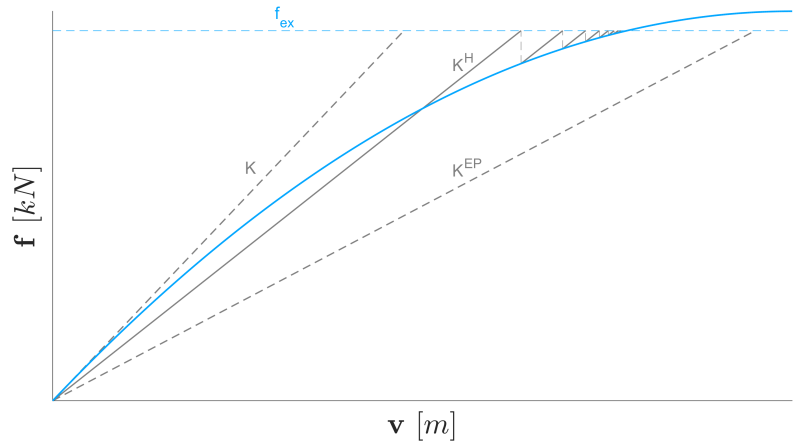

Figure 4.4: Hybrid iteration.

In order to solve this problem, a rather simple solution was implemented. Instead of replacing the elastic predictor completely with the EP predictor, a new (hybrid) stiffness matrix $\mathbf{E}^H$ was created with the average values of the elastic and EP stiffness matrices:

$$\mathbf{K}^H = 0.5\left(\mathbf{K} + \mathbf{K}^{EP}\right). \tag{4.6}$$

This concept is visualized in Figure 4.4. Not only will the calculation most likely converge to an answer with this solution, but it will also converge faster than with just the elastic predictor. It has to be noted that this solution has the intrinsic assumption that the EP predictor may only predict a slightly lower stiffness than in reality. If the stiffness is severely underestimated by the predictor, this solution will fail to work and convergence problems may still arise. This, however, seemed not to be the problem for any of the calculations during the process of this thesis.

5
VERIFICATION

The implementation of the HCA model in Plaxis was verified by comparing the calculation results with results from calculations made in Abaqus. The Abaqus implementation had already been validated by comparison with a large number of laboratory test results. The verification case consisted of a simulation of a single element test with triaxial test characteristics, as described in this chapter. First, the model parameters and boundary conditions are described, after which the results and conclusions are discussed.

5.1. MODEL PARAMETERS & BOUNDARY CONDITIONS

To see if the HCA model in Plaxis was implemented correctly, a reference case was provided by Dr Wichtmann. The test case was representation of a triaxial test using a single axi-symmetrical type element. The element had a height of 0.10 m and a width of 0.05 m. The symmetry axis was located at the left boundary. This boundary was normally fixed, as was the lower boundary. The right and upper boundaries were unconstrained, but were subject to static and cyclic loads (pseudo-static) throughout the calculation. A schematization of the test dimensions can be found in Figure 5.1. The test was performed in five phases: four phases in which the hypoplasticity model was used and an ultimate phase where the HCA model was used:

1. *Hypoplastic* – A uniformly distributed stress of $\sigma_x = -150$ kPa (compression)was applied at the right boundary and a stress of $\sigma_y = -300$ kPa was applied at the upper boundary. Hence, $p' = 200$ kPa and $q' = 100$ kPa. The deformations during this stage were neglected and also the void ratio was left unaltered at the original value of $e_0 = 0.828$.

2. *Hypoplastic* – In addition to the static stresses, a harmonic stress with an amplitude of $\sigma_1^{ampl} = 60$ kPa and a frequency of 1 Hz was applied at the upper boundary during 1 cycle (i.e. 1 second).

3. *Hypoplastic* – The same loading and time interval as in the second phase was applied, but this time the strain loop was recorded by activating the *Hypoplastic Recording* model.

4. The fourth phase contained a module which calculated the intermediate results, such as the amplitude of straining, primarily for plotting purposes in the case that the HCA phase had numerical errors.

5. *HCA* – The *HCA Explicit* model was used to calculate the strain accumulation during 100,000 load cycles.

The applied vertical stress during all five phases can also be seen in Figure 5.1. The material parameters for the hypoplasticity model and HCA model which were used can be seen in Table 5.1 and Table 5.2. The initial density[1] was $e = 0.828$.

[1] i.e. the density at the beginning of step one, after application of the confining pressure.

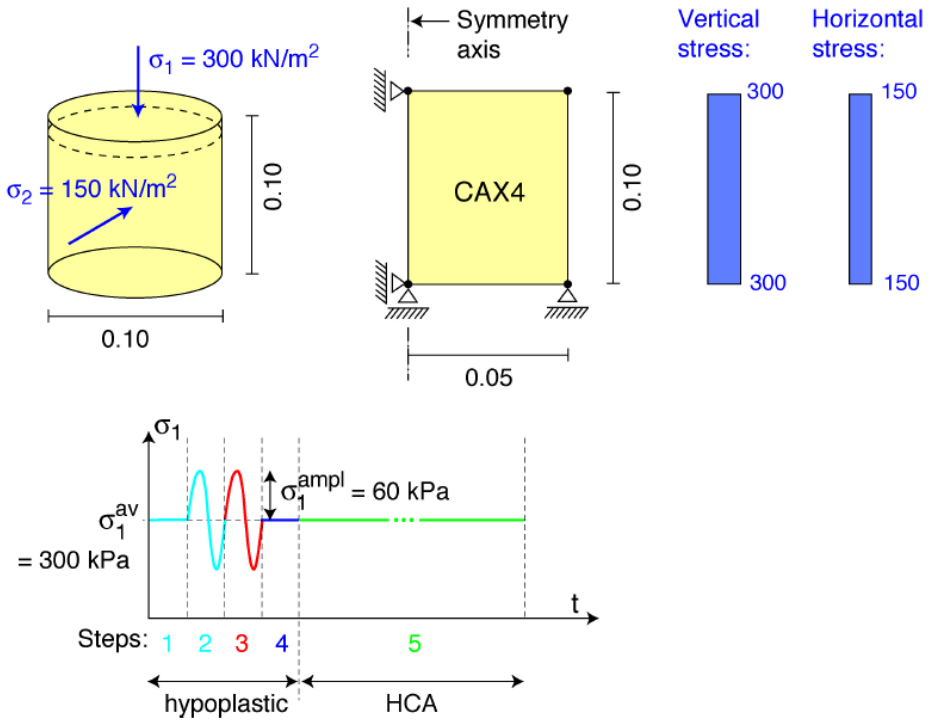

Figure 5.1: Schematic representation of verification case regarding boundary conditions and load characteristics.

φ_c [°]	ν [-]	e_{i0} [-]	e_{c0} [-]	e_{d0} [-]	h_s [MPa]	n [-]	α [-]	β [-]	R_{max} [-]	m_R [-]	m_T [-]	β_R [-]	χ [-]	h_{22} [-]
33.1	0.37	1.212	1.054	0.677	4000	0.27	0.14	2.5	10^{-4}	2.4	1.2	0.1	6.0	$1 \cdot 10^{-4}$

Table 5.1: Hypoplasticity input parameters for the triaxial verification case.

C_{N1} [-]	C_{N2} [-]	C_{N3} [-]	C_{ampl} [-]	C_e [-]	C_p [-]	C_Y [-]	e_{ref} [-]	A_K [-]	a_K [-]	n_K [-]	ν_{HCA} [-]
$2.95 \cdot 10^{-4}$	0.41	$1.90 \cdot 10^{-5}$	1.33	0.6	0.23	1.68	1.054	1209.0	1.63	0.50	0.32

Table 5.2: HCA input parameters for the triaxial verification case.

The verification case was performed in Plaxis 2D with the corresponding implementation of the hypoplasticity model and the HCA model. The input parameters were adopted from the Abaqus verification case and can be seen in Table 5.1 and Table 5.2. The same phases were applied in the Plaxis input program, except for phase 4, which was not available in the implementation at hand. This should not influence the result since no actual calculations were performed during this stage. No rectangular elements can be created in Plaxis, so two six-noded triangular axi-symmetrical elements were used to mimic the rectangular shaped sample. No time-dependency of the soil behaviour was expected, since the sample was assumed completely undrained. Therefore, a plastic calculation scheme was used. During the first phase, the deformations were not recorded, however neglecting the reduction in void ratio during a step is not possible in Plaxis. Therefore, the initial void ratio (at the beginning of step one) was increased to $e_0 = 0.850$ so that the void ratio at the beginning of step two was equal to 0.828. All other boundary conditions and state variables were considered equal. The results of the calculation can be seen in Figure 5.2. The angular shape of the strain curve during the first two load cycles is caused by the plastic calculation scheme. The angularity should not influence the result since the same strain path is followed as in the reference calculation.

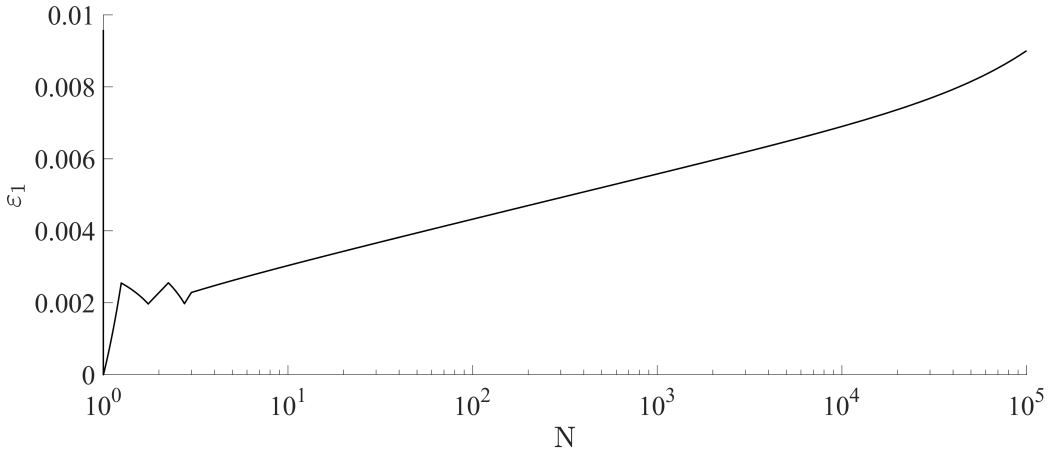

Figure 5.2: Strain accumulation results from Plaxis implementation.

5.2. RESULTS & CONCLUSIONS

The obtained parameters of interest were the amplitude of straining $\boldsymbol{\varepsilon}^{ampl}$ and the total axial strains obtained after one and 100,000 load cycles. Since the loading scheme and soil parameters were very homogeneous, the result should be mainly influenced by the boundary conditions and not by the interaction between the nodes (i.e. no redistribution of stress is to be expected). Therefore, the numerical integration method embedded in the software should not be of large influence as the calculations become relatively straightforward[2].

The results for the parameters of interest for both the reference and verification calculations can be found in Table 5.3. The resulting errors between the Plaxis and Abaqus implementation lay well below 0.5 % for all datapoints. These small errors can be well explained by the use of a slightly different initial density (0.01 % error) and numerical roundoff differences.

Preferably, more tests should be carried out with a variation in boundary conditions, initial conditions and output parameters such as the volumetric and deviatoric strain parts. Only by comparing a more extensive set of results from the two calculation methods, a confident conclusion can be drawn about the verification of the Plaxis implementation. Due to a lack of time and availability of such reference cases however, no additional verification calculations were made. Based on the results of the calculation that was made though, it was thought safe to assume that the constitutive equations of the HCA model were implemented correctly into Plaxis. It must however be kept in mind that a full verification requires an extensive amount of extra effort and time which should be carried out before the implementation can be used for any practical calculations. Such work was discontinued in this thesis for reasons of practicality.

	Reference $\cdot 10^{-3}$ [-]	Verification $\cdot 10^{-3}$ [-]	Error [%]
$\boldsymbol{\varepsilon}^{ampl}$	0.352	0.353	0.31
$\boldsymbol{\varepsilon}_1$(N=1)	-2.29	-2.28	0.31
$\boldsymbol{\varepsilon}_1$(N=1 $\cdot 10^5$)	-8.99	-9.01	0.16

Table 5.3: Results of the verification with the drained triaxial test case. The reference case was calculated in Abaqus and the verification case in Plaxis.

[2] In fact, a relatively simple Matlab script was written by the author of this thesis as reference which could accurately calculate the pseudo-creep phase of the problem at hand for a single integration point.

6

2D SHALLOW FOUNDATION CALCULATION

As previously mentioned, the constitutive equation of the HCA model was already validated with a series of drained cyclic triaxial tests. Also, a validation with the Abaqus FE implementation has been performed by recalculating the results of the centrifuge tests with a shallow foundation, as discussed in section 3.4. The necessity to perform additional validation in this thesis rises from the use of a different FE software package. It is important for the HCA model that the stress field and the strain paths at the end of the implicit phase are calculated as realistic as possible. Different FE software packages can have differences in modeling the interaction between elements in the mesh, leading to slightly different stress distributions and deformations. It is therefore evident to test the performance of the combination of the HCA model, the hypoplasticity model and Plaxis 2D FE software.

Wichtmann et al. have recalculated the centrifuge tests on a shallow foundation – mentioned in section 3.4 and thoroughly described in [15],[44] – to validate and calibrate the Abaqus HCA routine. In light of this thesis, the same recalculation was made with the Plaxis HCA routine. Next to the validation of the implementation, this has the additional advantage of comparing the results of Plaxis and Abaqus when given the exact same model and input parameters. An overview of the setup of the recalculation by Wichtmann et al. and its results can be seen in Figure 6.1.

6.1. MATERIAL CONSTANTS & BOUNDARY CONDITIONS

In the centrifuge tests of Helm et al. [44], a poorly-graded fine sand was used with $d_{50} = 0.21$ mm, $U = d_{60}/d_{10} = 2.0$, $\rho_s = 2.66$ g/cm^3, $e_{min} = 0.575$, $e_{max} = 0.908$. A set of material parameters for the hypoplasticity model with intergranular strain addition and the HCA model was derived for this sand in [15] and can be found in Table 6.1 and Table 6.2.

The following boundary conditions were applied to the Plaxis recalculation, based on the Abaqus recalculation in [15]:

- Strip foundation, therefore calculation as a problem with plane deformations. A drained plastic calculation scheme was used in all Plaxis calculation phases.
- dimensions of the test container: width 18.1 m, height 7.3 m (prototype). Using the symmetry only half of the soil was discretized (9.05 x 7.3 m).

φ_c [°]	ν [-]	e_{i0} [-]	e_{c0} [-]	e_{d0} [-]	h_s [MPa]	n [-]	α [-]	β [-]	R_{max} [-]	m_R [-]	m_T [-]	β_R [-]	χ [-]	h_{22} [-]
32.8	0.20	1.044	0.908	0.575	150	0.40	0.12	1.0	10^{-4}	3.9	1.85	0.2	6.0	$1 \cdot 10^{-4}$

Table 6.1: Hypoplasticity input parameters for the shallow foundation case.

C_{N1} [-]	C_{N2} [-]	C_{N3} [-]	C_{ampl} [-]	C_e [-]	C_p [-]	C_Y [-]	$\hat{\varepsilon}_{ref}$ [-]	A_K [-]	a_K [-]	n_K [-]	ν_{HCA} [-]
$1.1 \cdot 10^{-3}$	0.38	$5.3 \cdot 10^{-5}$	2.0	0.51	0.43	2.0	0.908	166.7	0.0	1.0	0.20

Table 6.2: HCA input parameters for the shallow foundation case.

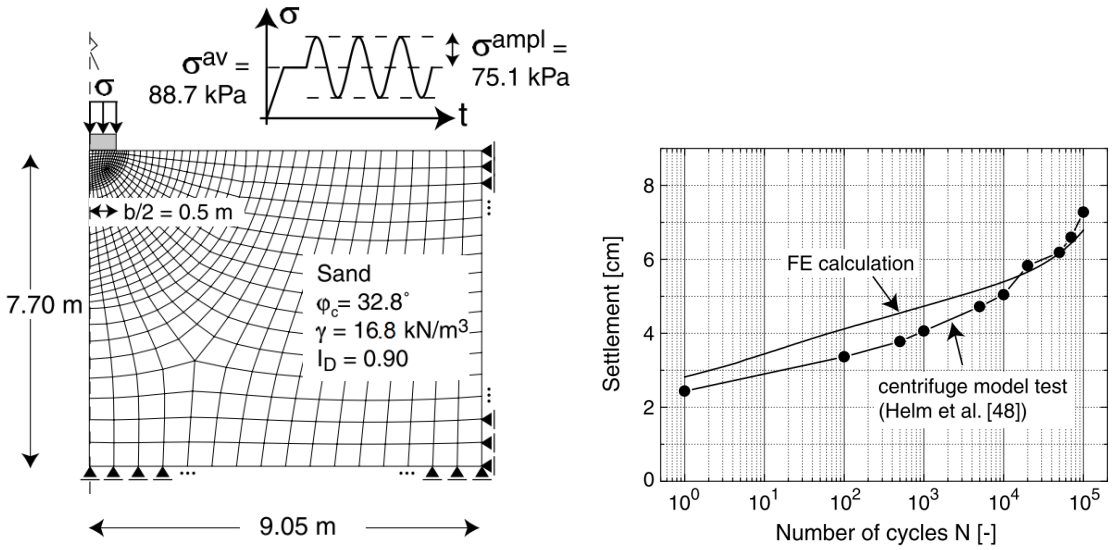

(a) (b)

Figure 6.1: FE calculation of a shallow strip foundation, where (a) displays the setup of the FE calculation in Abaqus and (b) shows the results in comparisson with the test results of the centrifuge test. [15].

- Foundation: width $b = 1.0$ m (only 0.5 m modeled due to symmetry), height $h = 0.6$ m, depth of embedding $t = 0$ m.
- Material model of foundation (aluminum): linear-elastic, unit weight $\gamma = 27$ kN/m^3, $E = 25$ GPa and $\nu = 0.3$.
- Average load $\bar{\sigma} = 89$ kPa, amplitude $\hat{\sigma} = 75$ kPa.
- Freshly pluviated sand, i.e. $g_0^A = 0$.
- Initial density $I_{D0} = 0.9$ ($e_0 = 0.608$; uniform).
- Coefficient of lateral pressure $K_0 = 1 - \sin(\varphi_P) = 1 - \sin(38°) = 0.38$.
- Initial value of the intergranular strain: component in the vertical direction $h_{11} = R$ due to pluviation, all other components zero.
- No back-polarization effects are taken into account.
- Parameters for virtual soil-structure interface layer: $E_{\text{oed}}^{\text{ref}} = 25$ GPa, $c'_{\text{ref}} = 0.1$ kPa, $\varphi' = 25.1°$, $\psi = 0°$, UD-power = 0, UD-P$^{\text{ref}} = 100$ kPa.
- Capillary suction parameter $p_t = 3.5$ kPa (for numerical stability; see section 6.4).

6.2. MESH DEPENDENCE

To determine the effect of the coarseness of the used mesh, a mesh dependence analysis was performed. Mesh refinements were applied to ensure that the mesh was finer in areas where stresses were larger. 6-nodal plane-strain type elements were used for all calculations. A higher number of elements is ought to lead to a higher accuracy of the result, but also increases the runtime of the calculation significantly. In Figure 6.3, the calculation results can be seen with the used number of elements. It can be seen that the influence on the result of the different kind of meshes is minimal. The coarsest mesh with 140 elements slightly underestimates the settlements after initial loading.

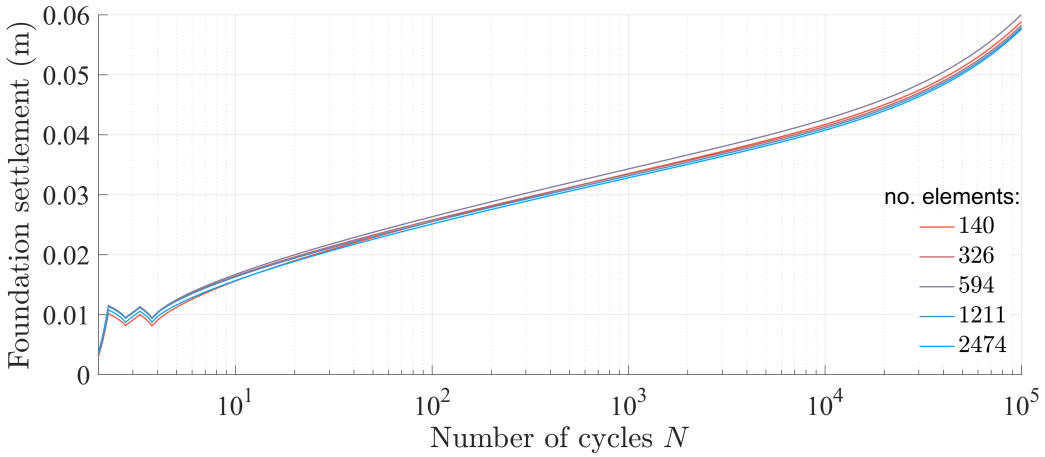

Figure 6.3: Results of the mesh dependence analysis. The lines are colour coded from coarse (red) to fine (cyan) meshes.

The meshes with more than 326 elements do not have this error. Interesting to see is that the result of the 326 and 1211-element meshes are closer together than the 594 mesh is with any of them. This indicates that the increase of elements does not linearly converge to an optimal result. Please note that slightly lower settlements were obtained in this analysis due to the use of a slightly different configuration of numerical stability parameters (see section 6.4).

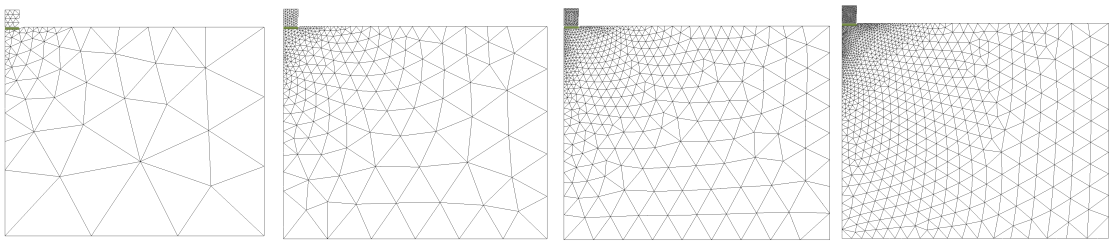

Figure 6.2: Different mesh refinements for the Plaxis calculation. From left to right: 140, 594, 1211, 2474 elements per mesh.

6.3. RESULTS

The evolution of foundation settlement (vertical component of translation) can be seen as the black line in Figure 6.4. Some key settlement values can also be found in the second column of Table 6.3. The settlements due to application of the own weight have been subtracted from the other settlements. It can be seen that the settlement after the first cycle corresponds fairly to the observed initial settlement in the centrifuge test. However, the foundation displacement amplitude and the final foundation settlement after 100.000 cycles are severely overestimated by almost a factor two.

In the dissertation of Wichtmann [15], also a larger displacement amplitude was observed initially and therefore, the values of m_R and m_T were increased to make the calculated values fit the observed ones. This method was also tried out in the Plaxis calculations, but the results were unsatisfactory. Adjusting the values to $m_R = 5.5, m_T = 2.0$ resulted in the grey line in Figure 6.4 Adjusting the values of m_R and m_T would not only decrease the settlement amplitude, but also the value of the settlement itself, which would make the result seem quite fabricated (which was actually true), even though the end result could be close to the values observed in the centrifuge test.

It is clear that the implicit phases (where the hypoplasticity model was used) have provided some erroneous results. The root cause of these errors seemed to be the result of the Plaxis 2D numerical scheme, as the Abaqus calculation provided more accurate results with similar model param-

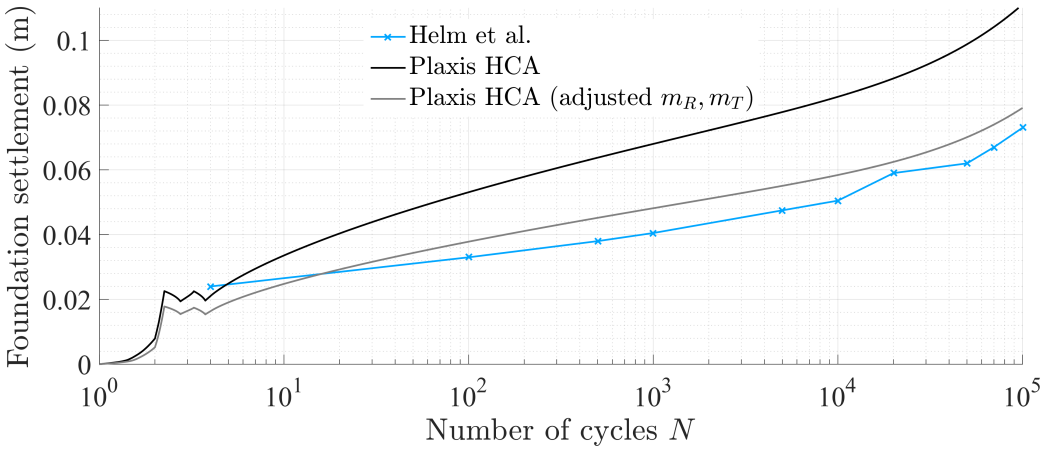

Figure 6.4: Foundation settlement results of the Plaxis 2D FE calculation, compared with the observed foundation settlements of the centrifuge test in Helm et al [44]. The grey line was calculated with $m_R = 5.5, m_T = 2.0$.

	Helm et al.	Plaxis FE	Abaqus FE
Settlement after:			
- Application of own weight [mm]	4	0.3	4
- First cycle [cm]	2.4	2.1	2.8
- 100.000 cycles [cm]	7.3	11.1	6.8
Displacement amplitude [mm]	0.8	1.45	0.86

Table 6.3: Observed results of the centrifuge test and the obtained results from both the Plaxis (with original parameters) and Abaqus (with adjusted m_T, m_R) recalculations.

eters and boundary conditions. Numerical instabilities were observed in the Plaxis calculation – described in section 6.4 – which could be the source of the errors.

6.4. NUMERICAL ISSUES

6.4.1. CONVERGENCE

During the initial recalculation of the 2D shallow foundation case, severe problems with convergence of the calculation were observed during iteration steps of the HCA model (pseudo-creep phase only). Strains of more than $1 \cdot 10^{10}$ were observed, so it seemed the calculation coped with divergence issues. Some other calculations regarding shallow foundations with different size and loading patterns were carried out, but the majority of these calculations was aborted due to similar divergence problems.

In her dissertation, Solf [39] also mentions some potential problems with the HCA implementation in Abaqus due to numerical convergence issues. She writes that inhomogeneities in stress state between neighboring elements or even within one element can arise due to relatively large local accumulation rates. These inhomogeneities are amplified by the stress dependent factor f_p, which provides a positive forward loop. Due to this mechanism, a single element may cause the FE calculation not to converge. For problems regarding shallow foundations, she recommends a 'quick-fix' by keeping the factor f_p in each element fixed to the value at the end of the second regular cycle. The values of f_p should be updated during regular control cycles. In problems involving piled foundations, such a solution does not suffice since the interaction stresses at the pile-soil interface are greatly influenced by the progression of accumulation. She recommends the application of reduced integration techniques for solving this problem. Also, in Niemunis (2005) [1] the application of elements with reduced integration is mentioned.

Elements with reduced integration are simply not available in the latest version of Plaxis during the writing of this thesis. The 'quick-fix' proposed by Solf of keeping the value of f_p fixed during the pseudo-creep phase was applied to some calculation cases regarding a shallow foundation, but unfortunately this approach was not able to prevent the calculation to abort due to convergence problems.

Another possible cause for problems with convergence in FE iteration schemes is the use of an erroneous elastic or elasto-plastic predictor (stifness matrix). With this in mind, the calculation routines for the elastic and elasto-plastic stiffness matrices were investigated. It was noticed that when the calculation of the elasto-plastic stiffness matrix was omitted (and the elastic one was used instead), the convergence issues were not observed during calculation. However, using the elastic predictor in situations where plasticity effects play a role might lead to large runtimes. To increase the speed of calculation a hybrid method was introduced, as described in section 4.3. After implementation of this method, the problem dit not reoccur.

6.4.2. DISCRETE LOADFUNCTION

Shallow foundation calculations – especially with the hypoplasticity model – can be prone to numerical instabilities. As already mentioned in section 6.3, numerical instabilities were observed in the Plaxis calculations. In section D.1, some examples can be seen of observed irregular stress and strain distributions underneath the foundation. In a closeup of the stress distribution near the foundation corner (see Figure D.3) it can be seen that the stress interaction between the foundation block and the underlying soil is not modelled correctly. The vertical stress underneath the block is decreasing towards the edge of the block, while in reality one would expect the stress to increase to a peak value at the edge, sine the block can be considered a stiff foundation. Just besides the block, stresses are expected to be zero since there is no overburden pressure to maintain stress equilibrium, but are calculated otherwise. It is known that numerical methods tend to have trouble in modeling such discrete step functions. The stress gradient at the location of the foundation corner is infinite, which is a concept that cannot be grasped correctly with a continuous mathematical solver. It is not uncommon that numerical calculations experience errors. The significance of the errors depends on the required degree of accuracy of the answer. In this case, it is thought that the numerical errors are indeed significant.

6.4.3. NUMERICAL TENSILE STRAINING

Small numerical errors can also cause another type of unrealistic straining. At the surface – or other areas with near zero stresses – small numerical errors can cause the calculation of small tensile stresses. Since granular materials have little or zero tensile strength, plastic deformations will be calculated, which is unrealistic. The hypoplasticity model, however, can prevent this from happening with the numerical parameter p_t which acts as a capillary suction in all integration points. As a guideline, it is advised to set p_t to a value just large enough to prevent tensile stresses in the near-zero-stress areas. The required value is dependent on the model boundary conditions. It is assumed intrinsically that the applied value of p_t will not influence the result significantly. The HCA model also has such an internal parameter, which is hard-coded as a fixed value of 0.1 kPa in the Fortran code of the model.

To make a proper comparison between the Plaxis and Abaqus calculations, the total set of model parameters should be as equal as possible. In both the publications [1] and [15] no taken measures were mentioned to prevent such numerical errors. Therefore, the value of p_t which was used in the calculations presented in [15] was requested from dr. Wichtmann, the first author of the publication. From his response it became clear that next to the parameter p_t, also an overburden pressure was applied to the soil surface next to the foundation. Unfortunately, the specific values of both p_t and the overburden pressure which were applied in the calculations were not documented properly. It

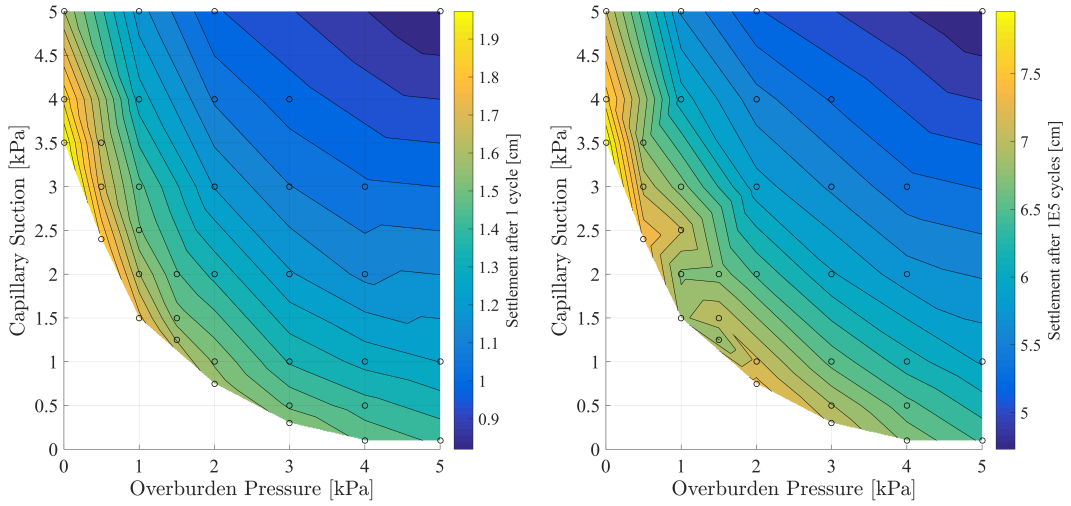

(a) (b)

Figure 6.5: The dependency of the calculation of accumulated settlement on a different choice of numerical stabilization parameters. The white zone represents the area where the calculation would fail due to numerical errors.

was however notified that the applied values had to be "below 5 kPa for both parameters".

An analysis was carried out to determine the sensitivity of the model to the aforementioned numerical stability measures, the results of which can be seen in Figure 6.5. The stabilization measures seem to have a remarkably significant influence on the result. By picking a random combination of values between 0 and 5 kPa for both measures, the resulting settlement could lie between approximately 5 and 8 cm. Even for the range of combinations which only just assured numerical stability (near the white zone in Figure 6.5), there remained a 1.5 cm spread in results.

It is questionable if both the numerical stability measures are actually necessary for shallow foundation calculations. A minimum value for the capillary pressure is required since below a value of 0.1 kPa, large defections were observed. However, for a minimum capillary pressure of 3.5 kPa, no overburden pressure was required to assure numerical stability. It is unclear if the overburden pressure has any physical significance. It could also not prevent the occurrence of numerical fluctuations in stress and strain underneath the foundation, as discussed in Figure D.4. Therefore, in the presented calculations in this thesis, the use of an overburden pressure was rejected and a capillary pressure in the hypoplasticity model of 3.5 kPa was chosen as a measure to prevent numerical instability.

6.5. PREDEFINED DISPLACEMENT BOUNDARY

In the previous calculation, the effect of the vibrating foundation was modeled as a distributed cyclic load to the soil surface. Another approach is to model the cyclic behaviour by applying a predefined distributed displacement to the soil surface at the location of the foundation. This could be done since the cyclic displacement trajectory of the foundation was known from the centrifuge test results. This approach was utilized in a second calculation, where the foundation block and cyclic distributed load were replaced by a rigid plate with zero weight which was given a forced cyclic vertical displacement according to the observed settlements of the centrifuge test by Helm et al. (the settlement amplitude and settlement after the first cycle were adopted from the first column of Table 6.2). The strain amplitudes in the soil were recorded in the recording phase while the rigid plate experienced the exact same settlement path as was observed in the centrifuge test. After the second cycle, the displacement boundary condition at the plate was once again replaced by a vertical

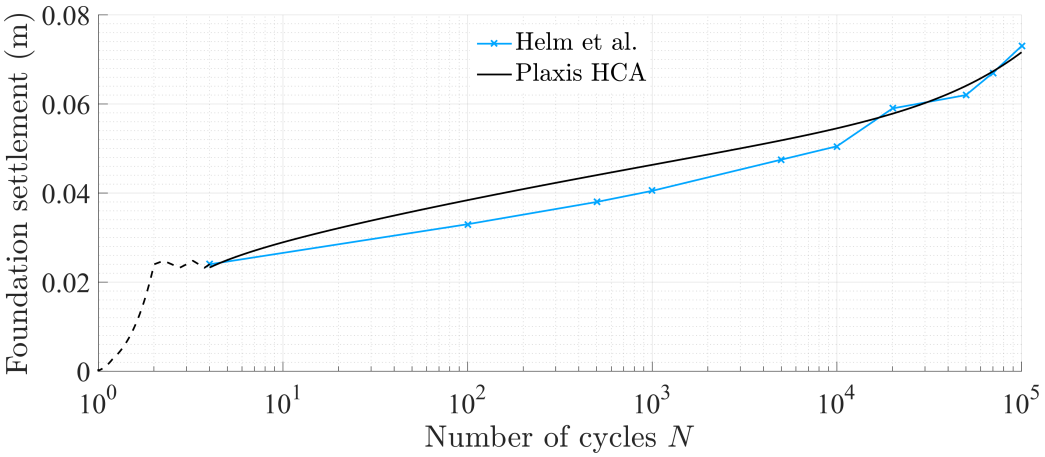

Figure 6.6: Results of the Plaxis 2D FE calculation with prescribed foundation displacements in the implicit phases, compared with the observed results from the centrifuge test of Helm et al.

static distributed load of 89 kPa, in accordance with the centrifuge test conditions. This replacement resulted in a 0.5 mm heave of the plate.

By following the above described calculation set-up, the recorded strain amplitudes, the soil densities and the stress state in the soil at the beginning of the pseudo-creep phase were ought to be very similar to the conditions in the real test. The results of this calculation can be seen in Figure 6.6. The progression of accumulated foundation displacement seems to coincide very well with the test results. This gives rise to believe that when the cyclic strain amplitudes in the soil are calculated correctly in the implicit phase, the HCA routine can provide results of high quality.

6.5.1. SENSITIVITY ANALYSIS

To get an idea of the sensitivity of the HCA procedure to its input values, a one-at-a-time (OAT) sensitivity analysis (adopted from [54]) was carried out, the results of which can be seen in Figure 6.7. Some of the parameters could not be chosen independent by definition or were otherwise strongly correlated to other parameters (see Appendix D). Many other input parameters of the hypoplasticity model and the HCA model have a correlation which is not so easily established in terms of mathematical rules. These correlations origin from their determination method by curve fitting of experimental results. For the sake of simplicity, these correlations have been neglected. Instead of the initial void ratio e_0, the initial relative density ($RD_0 = \frac{e_{max}-e_0}{e_{max}-e_{min}} \cdot 100\%$) was used in the sensitivity analysis. This was mainly to avoid unrealistic input scenario's (such as $e_0 < e_{min}$).

Each input parameter X was changed 5 %[1] up (X^+) and down (X^-) with respect to their standard value (X_0) in Table 6.1 and Table 6.2. The final settlements u were denoted, after which the values were set back to their standard value before continuing with the next parameter. The settlements were collected both after the first cycle and after 100.000 cycles. The sensitivity η_{SR} of each parameter X was defined as percentage change in output divided by the percentage change in input:

$$\eta_{SR} = \frac{\frac{u(X^{+,-})-u(X_0)}{u(X_0)}}{\frac{X^{+,-}-X_0}{X_0}} \tag{6.1}$$

A normalized value of the parameter sensitivity was obtained by estimating their input range (see

[1] A fixed low input range was chosen, primarily because a realistic range of possible values was not known for most parameters and secondly; because a too large range could lead to numerical instabilities.

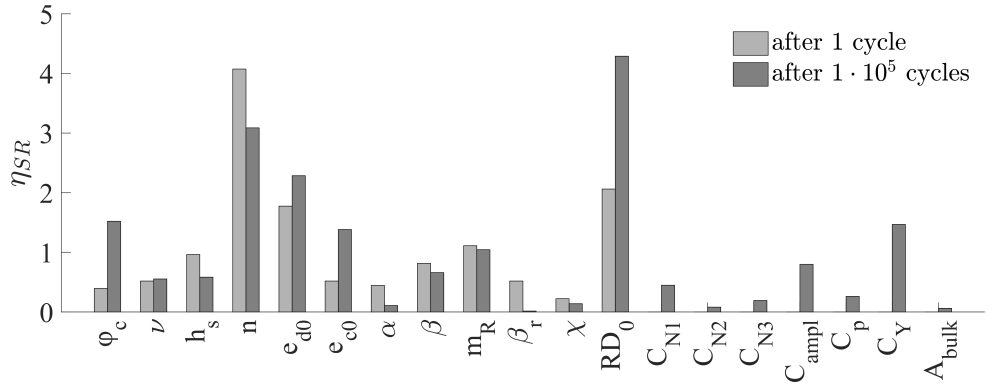

Figure 6.7: Relative sensitivity values η_{SR} of the investigated model parameters. A value of 1.0 means that a certain percentage change in input will lead to an equal percentage change in output.

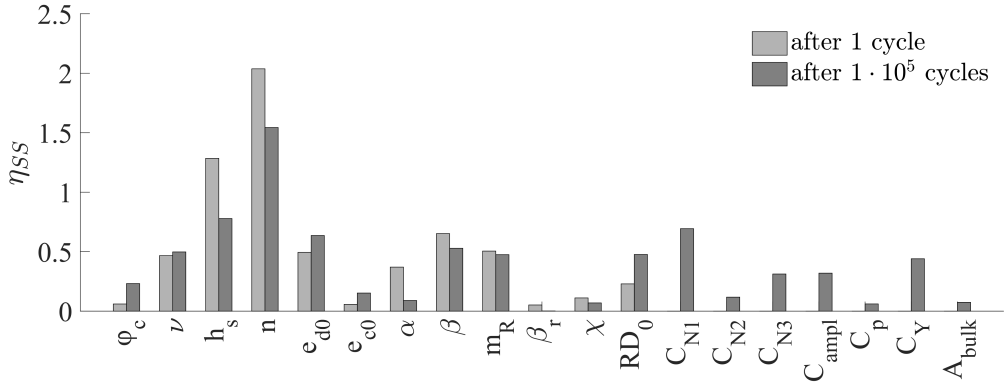

Figure 6.8: Sensitivity values η_{SS} of the investigated input parameters, normalized by their (approximated) input range.

Appendix D for an explanation) and normalizing the sensitivity with:

$$\eta_{SS} = \eta_{SR} \cdot \frac{X_{range}}{X_0} \tag{6.2}$$

It can be seen that the parameters of the hypoplasticity model are most influential on the results of the HCA routine. In particular, the h_s and n parameters stand out in Figure 6.8. This is in line with the findings from Anaraki [50], which concluded that the hypoplastic model is most sensitive for those parameters during soil compression. To put the sensitivity values of Figure 6.8 in perspective, one should bear in mind that the value of $\eta_{SS} \approx 0.5$ for m_R corresponds to the range and effect of m_R as indicated by the gray and black line in Figure 6.4.

6.6. CONCLUSIONS

In this section, the recalculation of the Helm et al. centrifuge test with the HCA routine in Plaxis 2D was discussed. It was observed that the HCA routine cannot provide an accurate prediction of the accumulated foundation settlements, since an overestimation of final settlements of almost factor two was calculated. The erroneous intermediate results and observed numerical errors amplify the doubts about the quality of the answer.

The large influence of numerical stabilization measures contributes to the doubts about the quality. The intrinsic assumption that the measures have little influence on the final result is untrue, since it was observed that seemingly insignificant changes can already lead to over 20% deviation in final settlement. Since these parameters are generally not thought of as influential parameters, this can lead to severe non-conservative errors. Therefore, a thorough investigation of the influence of these measures is advised in shallow foundation calculations with the HCA routine.

An improvement of quality can be expected when the (initial) cyclic settlement behaviour of the foundation is known. By ruling out the errors in initial settlement and settlement amplitude, the quality of the answer improved significantly.

It is also important to notice that the HCA model in combination with the hypoplasticity model with intergranular strain extension has an extensive amount of material parameters. The majority of these parameters cannot be accurately obtained with in-situ measurements, but should be determined with advanced laboratory tests. The importance of an accurate determination of all parameters was revealed in the sensitivity analysis. Especially the parameters of the hypoplasticity model were discovered to be most influential to the result.

7
CONCLUSIONS & RECOMENDATIONS

7.1. GENERAL
In this thesis, the high-cycle accumulation (HCA) model by Niemunis et al. was inspected and implemented in Plaxis 2D finite element (FE) software. The implementation was performed by converting a user-material (UMAT) routine for Abaqus into a user-defined soil model (UDSM) for Plaxis 2D in the Fortran programming language. Several calculations were performed to verify and validate the model implementation: a verification case of a cyclic triaxial test, which was obtained from one of the authors of the model and; a recalculation of a shallow foundation centrifuge test which is described in literature.

7.2. CONCLUSIONS
In light of the main objectives of this thesis:

- Increase the availability of the HCA routine to geotechnical engineers and scientist in The Netherlands.

- Identify the possibilities and limitations of applying the HCA model in a Plaxis finite element routine for a relevant engineering problem and formulate recommendations for future use.

the following main conclusions were drawn:

- The constitutive equations of the HCA routine were successfully implemented in a finite element routine in Plaxis 2D software and its workings were verified for the analysis of a drained cyclic triaxial test. For practical applications in 2D boundary condition calculations however, the current FE implementation seems unfit due to problems of numerical origin.

- For the design of shallow foundations, the use of the modified hypoplasticity model with intergranular strain (IGS) extension in Plaxis 2D to assess the initial conditions (strain amplitudes, initial strains, stress distribution) of the HCA model is not advised without validation, because:

  - The finite element routine – without an optimized numerical interface – seems unable to correctly model the large stress gradients near shallow foundation corners, which leads to incorrect predictions of the initial conditions.
  - The method of determining the material parameters for the hypoplastity model with IGS was proven to provide parameters which were incapable of accurately modeling the cyclic behaviour;
  - The method requires an impractical amount of laboratory work to determine the set of model parameters for both the hypoplasticity and the HCA model.

It must be noted that no effort was put in the optimization of the numerical interface in Plaxis 2D, since it was thought to require an extensive amount of work and understanding of the inner workings of the program. It may well be that better results can be obtained after such optimization.

- The quality of the accumulation prediction is much more promising when the deformation amplitude of the foundation is known and applied as a prescribed displacement in Plaxis 2D. It could therefore be thought that the prediction of future settlements of existing shallow foundations (of which the settlement amplitude can be measured) with the HCA routine in Plaxis 2D is a viable possibility. However, in such case there is still the largely unsolved problem of determining the in-situ cylic strain history.

- A sensitivity analysis showed that the HCA routine is most sensitive to the parameters of the hypoplasticity model, which actually shows that the HCA model is very sensitive to the calculated strains and strain amplitudes in the implicit phase. When looking at the constitutive model, it can be seen that the strain amplitude is a very influential parameter, so these observations are to be expected. It is therefore also expected that also for other boundary conditions and state parameters, the results of the implicit phase will be largely determining the final outcome of the model.

- The definition of the elasto-plastic stiffness tensor in the HCA constitutive model can lead to an underestimation of stiffness. This can cause severe divergence of the numerical calculation. A modification was proposed, which seems to remove this problem, though it must be noted that it is a rough solution.

- Based on the literature study, the application of the HCA model to engineering problems should be omitted if one of the following applies:

  - Multi-frequency loading;
  - Cyclic pre-loading;
  - An intermediate change in average load or overburden pressure;
  - Sequencing is of importance in case of irregular loading.

7.3. RECOMMENDATIONS

The following topics were outside the scope of this thesis, but were thought to be relevant topics for future research:

- The verification of the Plaxis HCA implementation should be extended by varying the input parameters (such as initial density, stress states etc.) and qualitatively comparing the outcome with expectations.

- It should be investigated whether an optimized numerical interface in Plaxis can provide a solution for the numerical issues at hand.

- The proposed method by Wichtmann [15] for determining the in-situ cyclic strain history should be worked out and validated to increase the applicability of the HCA model for existing structures.

- The elasto-plastic stiffness tensor in the HCA constitutive model should be investigated and possibly revised.

- It is thought that the method of determining the hypoplastic material parameters leaves room for subjective interpretation. An investigation to the objectivity of the parametric determination method is therefore advised.
- Long-term in-situ measurements at cyclically loaded civil structures should be performed to validate the HCA model for practical use.

A

SYMBOLS & NOTATIONS

In the course of this thesis, the following symbols and notations have been used:

A_ε	Tensorial strain amplitude
A_k	Material constant for elastic stiffness in HCA model
a_k	Material constant for elastic stiffness in HCA model
$C...$	Material constant
CSR	Cyclic shear-stress ratio
DR	Relative density
E	Young's modulus of elasticity
$\mathbf{E}$	Elastic stiffness tensor
$\mathbf{E}^{ep}$	Elasto-plastic stiffness tensor
e	Void ratio
e_{min}	Minimum void ratio
e_{max}	Maximum void ratio
$f...$	Scalar factor in the HCA constitutive model
g^A	Historical cyclic loading "memory"
I_{D0}	Initial density
K	Bulk modulus
L	Height (m)
M	Critical state line from Can-Clay flow rule
$\mathbf{m}$	Direction of accumulation
N	Number of cycles
$\tilde{\mathrm{N}}$	function of γ^{ampl} and N in Sawicki's model
n	Porosity
n_k	Material constant for elastic stiffness in HCA model
p	Isotropic stress state
p_{atm}	Atmosperic (reference) pressure
q	Deviatoric stress state
u	Vertical deformation (m)
γ	Shear strain
γ^{ampl}	Shear strain amplitude
ε	Strain
ε^{acc}	Accumulated plastic strain vector
ε^{ampl}	Strain amplitude (scalar)
$\hat{\varepsilon}$	Strain amplitude (scalar)
ε^e	Elastic part of straining
ε^{pl}	Plastic part of straining (for numerical implementation)

ε_{ref}	Reference strain amplitude
ν	Poisson's ratio
σ	Stress (kPa)
$\dot{\sigma}$	Stress rate
σ^{ampl}	Stress amplitude
Φ	Compaction

A superposed dot notation ($\dot{\_}$) refers to the rate with respect to the number of cycles ($\dot{\varepsilon} = \delta\varepsilon/\delta N$). Scalars are expressed in plain style (e), while vectors and tensors are expressed in bold style ($\boldsymbol{\varepsilon}, \mathbf{E}$). A multiplication with a colon : indicates a double contraction, which can be used to calculate the scalar product of two tensors. $\mathrm{tr}X$ reads the trace of tensor X and $\det X$ is the determinant. Furthermore, the following definitions have been adopted:

$$p = -(\sigma_1 + \sigma_2 + \sigma_3)/3; \quad q = -\sigma_1 + (\sigma_2 + \sigma_3)/2$$

$$I_1 = \mathrm{tr}\,\boldsymbol{\sigma}; \quad I_2 = [\boldsymbol{\sigma} : \boldsymbol{\sigma} - (\mathrm{tr}\,\boldsymbol{\sigma})^2]/2; \quad I_3 = \det \boldsymbol{\sigma}$$

B

MODIFICATIONS TO THE HYPOPLASTICITY MODEL

Next to the extension for intergranular strains, Niemunis also made some modifications to the original hypoplasicity model, as described in [15, 49, 51]. For details, reference is made to these papers. A short elaboration of the modified formulas is described below. The following sections are directly quoted from [15], except for equation numbers and citation references, which refer to relevant items in this report.

FACTOR f_d

"If the factor f_d after Equation 3.27) is applied some deformation paths may lead to an under-shooting of the lower bound e_d of the void ratio (Niemunis et al. [51]). In order to prevent this, Niemunis et al. [51] modified the factor f_d for $e < e_c$:

$$f_d = \left(\frac{e-e_d}{e_c-e_d}\right)^{\alpha} + \left[1-\left(\frac{e-e_d}{e_c-e_d}\right)^{\alpha}\right]^{z} \bar{f}_d \tag{B.1}$$

$$\bar{f}_d = -\frac{M_e^{(d)}(1+e)\sqrt{3} + M_T^{(d)} f_b f_e \sqrt{3}(3+a^2)}{M_T^{(d)} f_b f_e 3a} \tag{B.2}$$

$$M_T^{(d)} = -\frac{e_d}{h_s} n \left(\frac{3p}{h_s}\right)^{n-1} \qquad M_e^{(d)} = 1 \tag{B.3}$$

$M_T^{(d)}$ and $M_e^{(d)}$ are the components of a vector perpendicular to the yield surface. The exponent $z = 5$ delivers an improved numerical stability."

INCREASED SHEAR STIFFNESS

"Niemunis [49] demonstrated that the original version of the hypoplastic model [...] exhibits a too low shear stiffness for the case of shear deformations near the p-axis. In a re-calculation of a cyclic undrained shearing, a much too fast build-up of pore water pressure was obtained [...]. The extension of the intergranular strain [...] cannot solve this problem [49].

In order to improve the constitutive equation Niemunis [49] proposed a modification of the shear stiffness. The Poisson's ratio ν was introduced as another material constant (original version $\nu = 0.38$ is too large). The modified stiffness tensor $\mathbf{L}_n$ reads:

$$\mathbf{L}_n = \mathbf{L} + f_b f_e \frac{1}{\hat{\mathbf{T}} : \hat{\mathbf{T}}} \left[\frac{\left(1+\frac{a^2}{3}+\frac{a}{\sqrt{3}}\right)(1-2\nu)}{1+\nu} - 1\right](I - \frac{1}{3}1\otimes 1). \tag{B.4}$$

The flow rule [...] was maintained. Thus, the nonlinear stiffness $\mathbf{N}$ had to be adapted:

$$\mathbf{N}_n = \mathbf{L}_n : \left(\mathbf{L}^{-1} : \mathbf{N}\right)" \tag{B.5}$$

C
FE IMPLEMENTATION

UMAT Argument	Description
stress	Cauchy stress tensor
statev	List of state variables
ddsdde	Stiffness tensor
stran	Strain tensor
dstran	Incremental strain tensor
time	Time at begin of step
dtime	Time increment during step
ntens	Dimensions of strain and stress tensors
nstatv	Number of state variables in *statev*
props	List of material properties
nprops	Number of material properties in *props*
coords	Spatial coordinates of integration point
drot	Rotational tensor
noel	Element number
npt	Local integration point number
kstep	Step number
kinc	Iteration number

Table C.1: Most important arguments for the Abaqus UMAT subroutine.

UDSM Argument	Description
IDTask	Plaxis calculation task number
iMod	Model number (in case of multiple UDSM's)
IsUndr	Defines drained/undrained conditions
iStep	Step number
iTer	Iteration number
iEl	Element number
Int	Local integration point number
X,Y,Z	Spatial coördinates of integration point
Time0	Time at begin of step
dTime	Time increment during step
Props	List of material properties
Sig	Cauchy stress tensor at end of step
Swp	Pore water pressure at end of step
StVar	List of state variables at end of step
**0*	Value of argument * at beginning of step
dEps	Incremental strain tensor
D	Stiffness tensor
BulkW	Bulk stiffness of water
nStat	Number of state variables is *StVar*

Table C.2: Most important arguments for the Plaxis UDSM subroutine.

Entry	Value	Entry	Value	Entry	Value
1	MOD Select	16	K_w [-]	31	C_{Y1} [-]
2	φ_c [°]	17	e_0 [-]	32	C_{Y2} [-]
3	p_t [kPa]	18	IS_{11} [-]	33	$C_{\pi 1}$ [-]
4	h_s [kPa]	19	IS_{22} [-]	34	$C_{\pi 2}$ [-]
5	n [-]	20	IS_{33} [-]	35	$C_{\pi 3}$ [-]
6	e_{d0} [-]	21	IS_{12} [-]	36	p_{atm} [kPa]
7	e_{c0} [-]	22	IS_{13} [-]	37	e_{ref} (=e_{c0}) [-]
8	e_{i0} [-]	23	IS_{23} [-]	38	Reference ampl. [-]
9	α [-]	24	C_{N1} [-]	39	-
10	β [-]	25	C_{N2} [-]	40	A_K [-]
11	m_R [-]	26	C_{N3} [-]	41	a_K [-]
12	m_T [-]	27	C_{ampl} [-]	42	n_K [-]
13	R_{max} [-]	28	C_e [-]	43	ν_{HCA} [-]
14	β_R [-]	29	C_{p1} [-]	44	$\varphi_{c,HCA}$ [°]
15	χ [-]	30	C_{p2} [-]		

Table C.3: Material properties array, assigned in the Plaxis Input material menu.

Entry	Value	Entry	Value
1-6	Inter granular strain parameters $IS_{\#\#}$	28	f_e
7-12	Strain tensor ε_0	29	$fffff$
13	Current void ratio e	30-111	Amplitude tensor
14	Neg. pore pressure	112	Debugging
15	Average stress	113	Closed loop flag
16	nfev	114	Epsamp: Strain amplitude
17	φ_{mob}	115	LoopN
18	ρ	116	g_0^A
19	dtsub	117	g^A
20	Numerical stability pressure	118	$\dot{g}^A$
21	sfi(t)	119-200	Backpolarization tensor π
22	intg	201-206	**m**: Direction of straining
23	f_{ampl}	207	F_m
24	g_{calc}	208	M
25	$N_1 \cdot N_3$	209	$\bar{Y}$
26	f_Y	210-270	Recorded strain loop
27	f_p		

Table C.4: Entries in the state variables array. Contains mostly function values for intermediate plotting, debugging parameters and storage of large vectors.

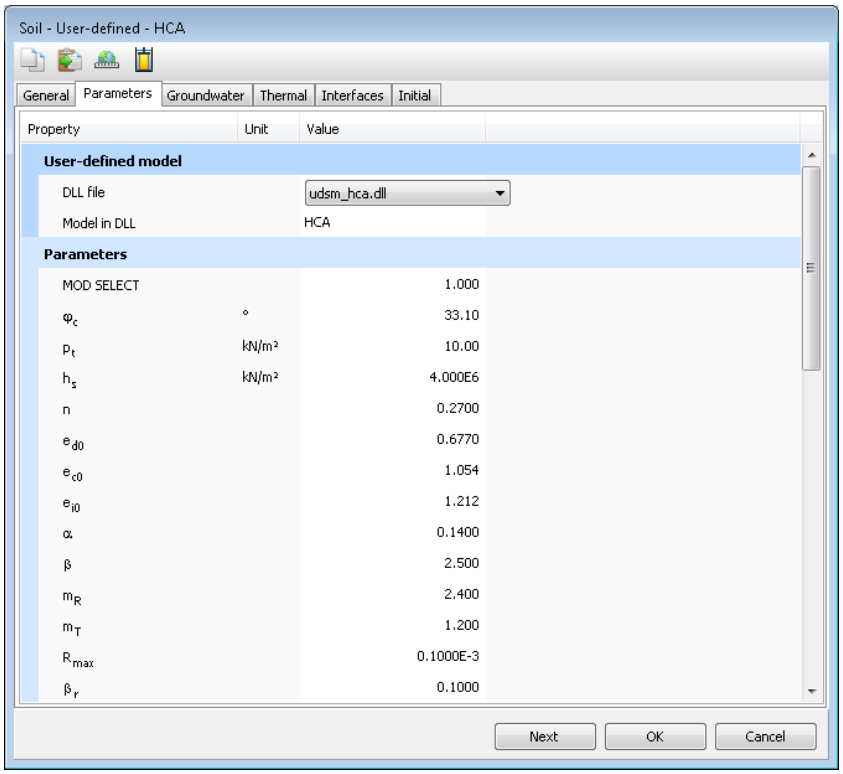

Figure C.1: Plaxis material properties input screen.

D

SHALLOW FOUNDATION CALCULATIONS

D.1. CALCULATION RESULTS

Figure D.1: Vertical Stress distribution after the first load peak on the foundation (164 kPa)

Figure D.2: Detailled close-up of the vertical stress distribution near the foundation corner in Figure D.1

Figure D.3: Distribution of vertical displacements at the foundation.

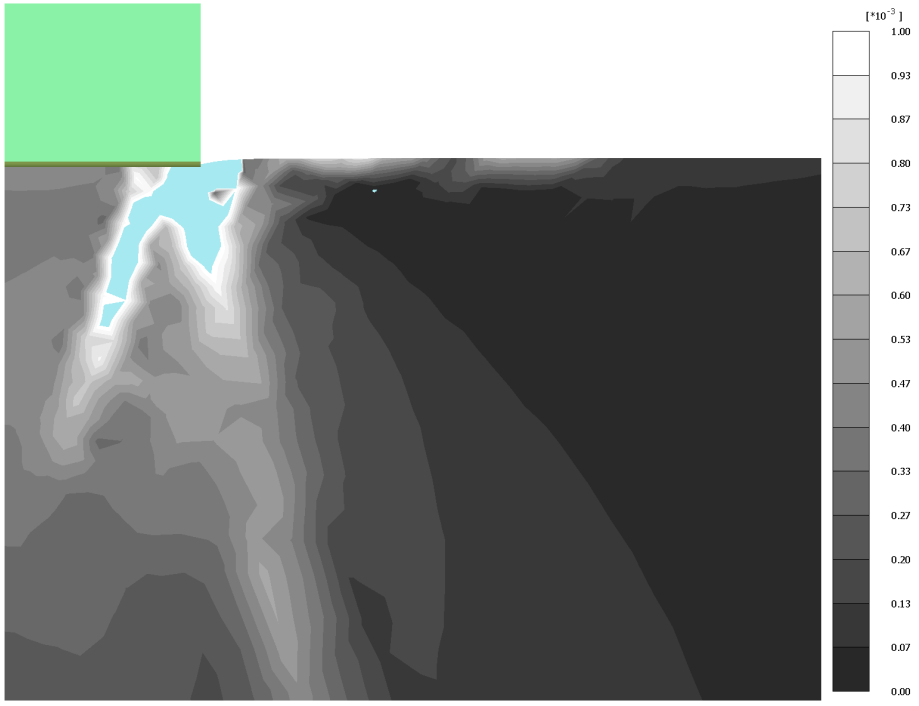

Figure D.4: Closeup of the recorded strain amplitude $\boldsymbol{\varepsilon}^{ampl}$ beneath the foundation. The gray scale color indication was cut off at a maximum of 1E-3. In the blue zone, higher strain amplitudes were recorded (with a maximum of 17E-3).

D.2. SENSITIVITY ANALYSIS

For the parametric sensitivity analysis in subsection 6.5.1, the following correlations between the parameters were adopted:

- $e_{i0} = e_{c0} \cdot 1.15$
- $m_R = 0.37 \cdot m_T$
- $e_0 = e_{d0} + (1 - RD_0) \cdot (e_{c0} - e_{d0})$
- $C_e = 0.89 \cdot e_{d0}$
- $e_{ref} = e_{c0}$

A range of parameter values was estimated to normalize the η_{SR} values and obtain the η_{SS} values. The selected ranges can be seen in Table D.1. The range estimations for the parameters ϕ_c and RD_0 were based on general engineering insight. The ranges of e_{d0} and e_{c0} were based on the results of a comparison between void ratio limits determination methods, presented in [7] and subsection 3.3.2. The DIN method turned out to provide relatively high void ratio values with respect to other methods that tested the same sand. The data of the research was used to determine the range of void ratio limits that could have been measured, had a different standard method than DIN been used. The ranges of the HCA parameters were determined by comparing the values from Wichtmann [15] with values calculated with the simplified parameter determination method (see subsection 3.3.1). The rest of the parameters ranges were estimated by analyzing the data sets for sands in [1, 15, 55].

Parameter	Range
ϕ_c [°]	30 – 35
ν	0.2 – 0.38
h_s [MPa]	100 – 300
n	0.3 – 0.5
e_{d0}	0.42 – 0.58
e_{c0}	0.83 – 0.93
α	0.1 – 0.2
β	0.8 – 1.6
m_R	3.0 – 5.5
β_r	0.19 – 0.21
χ	3.0 – 6.0
RD_0	0.85 – 0.95
C_{N1}	$0.5 \cdot 10^{-3}$ – $2.2 \cdot 10^{-3}$
C_{N2}	0.05 – 0.60
C_{N3}	$1.4 \cdot 10^{-5}$ – $1.0 \cdot 10^{-4}$
C_{ampl}	1.3 – 2.1
C_p	0.4 – 0.5
C_Y	1.7 – 2.3
A_{bulk} [MPa]	100 – 300

Table D.1: Estimated ranges for parameters in the sensitivity analysis of the shallow foundation HCA calculation.

BIBLIOGRAPHY

[1] A. Niemunis, T. Wichtmann, and T. Triantafyllidis, *A high-cycle accumulation model for sand,* Comput. Geotech. **32**, 245 (2005).

[2] T. Wichtmann, A. Niemunis, and T. Triantafyllidis, *On the determination of a set of material constants for a high-cycle accumulation model for non-cohesive soils,* Int. J. Numer. Anal. Methods Geomech. **34**, 409 (2009).

[3] A. Niemunis and T. Wichtmann, *Separation of time scales in the HCA model for sand,* Acta Geophys. **62**, 1127 (2014).

[4] A. Niemunis, T. Wichtmann, and T. Triantafyllidis, *On the definition of the fatigue loading for sand,* in *Int. Work. Const. Model. - Dev. Implementation, Eval. Appl.* (2007).

[5] T. Wichtmann, A. Niemunis, T. Triantafyllidis, and M. Poblete, *Correlation of cyclic preloading with the liquefaction resistance,* Soil Dyn. Earthq. Eng. **25**, 923 (2005).

[6] T. Wichtmann, *New findings regarding the behaviour of soils under cyclic loading,* (2016).

[7] Ø. Blaker, T. Lunne, T. Vestgården, L. Krogh, N. V. Thomsen, J. J. M. Powell, and C. F. Wallace, *In situ and laboratory testing Method dependency for determining maximum and minimum dry unit weights of sands,* Front. Offshore Geotech. III , 978 (2015).

[8] T. Wichtmann and T. Triantafyllidis, *Inspection of a high-cycle accumulation model for large numbers of cycles (N=2 million),* Soil Dyn. Earthq. Eng. **75**, 199 (2015).

[9] I. Herle and G. Gudehus, *Determination of parameters of a hypoplastic constitutive model from properties of grain assemblies,* Mech. Cohesive-Frictional Mater. **4**, 461 (1999).

[10] T. Meier, *Application of Hypoplastic and Viscohypoplastic Constitutive Models for Geotechnical Problems,* (2007).

[11] H. Fuchs and I. Stephens, *Metal fatigue in engineering* (Wiley, New York, 1980).

[12] J. Lemaitre and J. Chaboche, *Mechanics of solid materials* (Cambridge University Press, Cambridge, 1994).

[13] D. V. Okur and a. Ansal, *Stiffness degradation of natural fine grained soils during cyclic loading,* Soil Dyn. Earthq. Eng. **27**, 843 (2007).

[14] M. Kalinowska and M. Jastrzębska, *Behaviour of Cohesive Soil Subjected to Low-Frequency Cyclic Loading in Strain-Controlled Tests,* Stud. Geotech. Mech. **36** (2015), 10.2478/sgem-2014-0024.

[15] T. Wichtmann, *Explicit accumulation model for non-cohesive soils under cyclic loading,* Ph.D. thesis (2005).

[16] R. D. Barksdale, *Laboratory Evaluation of Rutting in Base Course Materials.* in *Proc. THIRD Int. Conf. Struct. Des. Asph. PAVEMENTS.* (London, 1972) pp. 161–174.

[17] M. Abdelkrim, G. Bonnet, and P. de Buhan, *A computational procedure for predicting the long term residual settlement of a platform induced by repeated traffic loading,* Comput. Geotech. **30**, 463 (2003).

[18] A. S. J. Suiker and R. de Borst, *A numerical model for the cyclic deterioration of railway tracks,* Int. J. Numer. Methods Eng. **57**, 441 (2003).

[19] F. Lekarp and A. Dawson, *Modelling permanent deformation behaviour of unbound granular materials,* Constr. Build. Mater. **12**, 9 (1998).

[20] F. Allou, C. Chazallon, and P. Hornych, *A numerical model for flexible pavements rut depth evolution with time,* Int. J. Numer. Anal. Methods Geomech. **31**, 1 (2007), arXiv:nag.2347 [10.1002] .

[21] A. Sawicki, *Engineering model for compaction of sand under cyclic loading,* Rozpr. Inz. **35**, 677 (1987).

[22] S. François, C. Karg, W. Haegeman, and G. Degrande, *A numerical model for foundation settlements due to deformation accumulation in granular soils under repeated small amplitude dynamic loading,* Int. J. Numer. Anal. Methods Geomech. **32**, n/a (2009), arXiv:nag.2347 [10.1002] .

[23] T. Wichtmann, a. Niemunis, and T. Triantafyllidis, *Validation and Calibration of a High-Cycle Accumulation Model Based on Cyclic Triaxial Tests on Eight Sands,* Soils Found. **49**, 711 (2009).

[24] T. Wichtmann, a. Niemunis, and T. Triantafyllidis, *Experimental evidence of a unique flow rule of non-cohesive soils under high-cyclic loading,* Acta Geotech. **1**, 59 (2006).

[25] C. Pasten, H. Shin, and J. C. Santamarina, *Long-Term Foundation Response to Repetitive Loading,* J. Geotech. Geoenvironmental Eng. **140**, 04013036 (2014).

[26] V. A. Diyaljee and G. P. Raymond, *Repetitive load deformation of cohesionless soil,* J. Geotech. Geoenvironmental Eng. **108** (1982).

[27] G. Gidel, P. Hornych, J. J. Chauvin, D. Breysse, and A. Denis, *A new approach for investigating the permanent deformation behaviour of unbound granular material using the repeated load triaxial apparatus,* Bull. Lab. Bridg. Roads **233**, 5 (2001).

[28] R. W. Lentz and G. Y. Baladi, *Constitutive equation for permanent strain of sand subjected to cyclic loading,* Transp. Res. Rec. **810**, 50 (1981).

[29] G. T. H. Sweere, *Unbound granular bases for roads,* Ph.D. thesis, Delft University of Technology (1990).

[30] S. F. Brown, *Repeated load testing of a granular material,* J. Geotech. Eng. Div. **100**, 825 (1974).

[31] G. Bouckovalas, R. V. Whitman, and W. A. Marr, *Permanent Displacement of Sand With Cyclic Loading,* J. Geotech. Eng. **110**, 1606 (1984).

[32] W. S. Kaggwa, J. R. Booker, and J. P. Carter, *Residual strains in calcareous sand due to irregular cyclic loading,* J. Geotech. Eng. **117**, 201 (1991).

[33] A. Sawicki and a. N. D. W. Swidzinski, *Mechanics of a Sandy Subsoil Subjected To Cyclic Loadings,* Int. J. Numer. Anal. Methods Geomech. **13** (1989).

[34] H. B. Seed and K. L. Lee, *Liquefaction of Saturated Sands During Cyclic Loading,* J. Soil Mech. Found. Div. **92**, 105 (1966).

[35] H. Matsuoka and T. Nakai, *A new failure criterion for soils in three-dimensional stresses.* (1982).

[36] T. Wichtmann, A. Niemunis, and T. Triantafyllidis, *Flow rule in a high-cycle accumulation model backed by cyclic test data of 22 sands,* Acta Geotech. **9**, 695 (2014).

[37] T. Triantafyllidis, T. Wichtmann, and a. Niemunis, *On the determination of cyclic strain history,* Int. Conf. Cycl. Behav. Soils Liq. Phenomena, 31 March - 02 April , 321 (2004).

[38] T. Wichtmann, a. Niemunis, and T. Triantafyllidis, *Improved simplified calibration procedure for a high-cycle accumulation model,* Soil Dyn. Earthq. Eng. **70**, 118 (2015).

[39] O. Solf, *Zum mechanischen Verhalten von zyklisch belasteten Offshore-Grundungen*, Ph.D. thesis, Karlsruhe Instutut fuer Technologie (2011).

[40] DIN, *18126 - Determination of Minimum and Maximum Dry Densities of non-cohesive soil,* (1996).

[41] T. Wichtmann, a. Niemunis, and T. Triantafyllidis, *Towards the FE prediction of permanent deformations of offshore wind power plant foundations using a high-cycle accumulation model,* , 635 (2011).

[42] R. Galindo, M. Illueca, and R. Jimenez, *Permanent deformation estimates of dynamic equipment foundations: Application to a gas turbine in granular soils,* Soil Dyn. Earthq. Eng. **63**, 8 (2014).

[43] T. Wichtmann, H. a. Rondón, a. Niemunis, T. Triantafyllidis, and a. Lizcano, *Prediction of Permanent Deformations in Pavements Using a High-Cycle Accumulation Model,* J. Geotech. Geoenvironmental Eng. **136**, 728 (2010).

[44] J. Helm, J. Laue, and T. Triantafydillis, *Untersuchungen an der RUB zur Verformungsentwicklung von B"oden unter zyklischen Beanspruchungen,* in *Boden unter fast zyklischer Belastung Erfahrungen und Forschungsergebnisse*, edited by T. Triantafyllidis (Bochum, 2000) pp. 109–133.

[45] T. Wichtmann, A. Niemunis, and T. Triantafyllidis, *On the "elastic" stiffness in a high-cycle accumulation model for sand: a comparison of drained and undrained cyclic triaxial tests,* Can. Geotech. J. **47**, 791 (2010).

[46] D. Masin, *PLAXIS implementation of HYPOPLASTICITY*, Tech. Rep. (2012).

[47] P.-A. von Wolffersdorff, *A hypoplastic relation for granular materials with a predefined limit state surface,* Mech. Cohesive-frictional Mater. **1**, 251 (1996).

[48] A. Niemunis and I. Herle, *Hypoplastic model for cohesionless soils with elastic strain range,* Mech. Cohesive-frictional Mater. **2**, 279 (1997).

[49] A. Niemunis, *Extended hypoplasticity models for soils,* in *Schriftenr. des Institutes fur Grundbau und Bodenmechanik der Ruhr-Universitat Bochum* (2003).

[50] K. E. Anaraki, *Hypoplasticity Investigated Parameter Determination and Numerical Simulation,* (2008).

[51] A. Niemunis, C. Karcher, and T. Theile, *An averaging procedure for layered materials,* Int. J. Numer. Anal. Methods Geomech. **24**, 837 (2000).

[52] Simulia, *Writing a UMAT or VUMAT,* Abaqus , 1.

[53] R. B. J. Brinkgreve, E. Engin, and W. M. Swolfs, *Material Models Manual,* Plaxis 2015 , 202 (2015).

[54] R. Brinkgreve, *Scientific Manual,* Plaxis (2011).

[55] J. Dijkstra, W. Broere, and O. M. Heeres, *Numerical simulation of pile installation,* Comput. Geotech. **38**, 612 (2011).